SARS-CoV-2 sensing by RIG-I and MDA5 links epithelial infection to macrophage inflammation

Lucy G Thorne[1,2] *, Ann-Kathrin Reuschl[1,2], Lorena Zuliani-Alvarez[1,2], Matthew V.X. Whelan[1,2], Jane Turner[1], Mahdad Noursadeghi[1], Clare Jolly[1,3,*], Greg J Towers[1,3,4*].

1. University College London, Division of Infection and Immunity, University College London, 90 Gower St, London WC1E 6BT, United Kingdom.

2. These authors contributed equally.

3. These authors contributed equally.

4. Lead Contact.

*Correspondance: g.towers@ucl.ac.uk, c.jolly@ucl.ac.uk, l.thorne@ucl.ac.uk

Keywords: SARS-CoV-2, inflammation, RNA sensing, epithelial, macrophage

Summary:

SARS-CoV-2 induces a robust, delayed innate immune response in airway epithelial cells, driven by activation of RNA sensors, which propagates inflammation through macrophage activation.'

Key points:

- SARS-CoV-2 activates RNA sensors and consequent inflammatory responses in lung epithelial cells.
- Epithelial RNA sensing responses drive pro-inflammatory macrophage activation.
- Exogenous inflammatory stimuli exacerbate responses to SARS-CoV-2 in both eplithelial cells and macrophages.
- Immunomodulators inhibit RNA sensing responses and consequent macrophage inflammation.

Abstract

SARS-CoV-2 infection causes broad-spectrum immunopathological disease, exacerbated by inflammatory co-morbidities. A better understanding of mechanisms underpinning virus-

associated inflammation is required to develop effective therapeutics. Here we discover that SARS-CoV-2 replicates rapidly in lung epithelial cells despite triggering a robust innate immune response through activation of cytoplasmic RNA-sensors RIG-I and MDA5. The inflammatory mediators produced during epithelial cell infection can stimulate primary human macrophages to enhance cytokine production and drive cellular activation. Critically, this can be limited by abrogating RNA sensing, or by inhibiting downstream signalling pathways. SARS-CoV-2 further exacerbates the local inflammatory environment when macrophages or epithelial cells are primed with exogenous inflammatory stimuli. We propose that RNA sensing of SARS-CoV-2 in lung epithelium is a key driver of inflammation, the extent of which is influenced by the inflammatory state of the local environment, and that specific inhibition of innate immune pathways may beneficially mitigate inflammation-associated COVID-19.

42 **Introduction**

43 SARS-CoV-2 has caused a devastating pandemic, >74.8 million confirmed cases, >1.6 million
44 deaths (https://covid19.who.int/, 20th December 2020) and a worldwide economic crisis.
45 Infection causes a remarkably wide, but poorly understood, disease spectrum, ranging from
46 asymptomatic (Allen *et al*, 2020; Treibel *et al*, 2020) to severe acute respiratory distress
47 syndrome, multi-organ failure and death (Docherty *et al*, 2020; Zhou *et al*, 2020).

48

49 The success of immunosuppressive corticosteroid dexamethasone in treating COVID-19 (Beigel
50 *et al*, 2020) suggests the importance of immunopathology in disease, likely driven by immune
51 activation in infected and virus-exposed cells. Intracellular innate immune responses have
52 evolved to detect and suppress invading pathogens, but inappropriate responses can also
53 contribute to disease (Blanco-Melo *et al*, 2020; Park & Iwasaki, 2020). Pathogen associated
54 molecular patterns (PAMPs) are detected by pattern recognition receptors (PRR), including
55 cytoplasmic nucleic acid sensors, and Toll-like receptors (TLR) that sample extracellular and
56 endosomal space. PRR activation triggers signaling cascades which activate downstream
57 transcription factors, including interferon (IFN) regulatory factors (IRFs) and NF-κB family
58 members, to initiate a defensive pro-inflammatory gene expression programme, principally
59 mediated by IFN secretion from infected cells. Paracrine and autocrine IFN signalling can suppress
60 viral replication and spread and, together with other secreted cytokines and chemokines,
61 coordinates adaptive immune responses. Viruses have evolved countermeasures to innate
62 defences and deploy a combination of evasion, and direct innate immune pathway antagonism,
63 to promote replication (Sumner *et al*, 2017). The resulting virus-host conflict is often a significant
64 cause of pathogenesis with PRR-induced inflammation driving disease at the site of replication
65 and systemically (Park & Iwasaki, 2020).

66

67 Missense mutations in innate immune pathways (Pairo-Castineira *et al*, 2020; Zhang *et al*, 2020),
68 and autoantibodies leading to deficient Type 1 IFN responses (Bastard *et al*, 2020), are associated
69 with severe COVID-19 suggesting that intact innate immune responses are important in
70 preventing disease, probably through controlling viral replication. Co-morbidities linked to severe

71 disease are typically inflammatory in nature suggesting that certain types of pre-existing
72 inflammation influence disease severity (Paranjpe *et al*, 2020). However the specific host-
73 pathogen interactions that cause disease, and how these are impacted by existing inflammation,
74 are not understood. Identification of the molecular events that link viral replication to
75 inflammation and disease will be critical in the development of novel and more precise
76 therapeutic agents. Moreover, such new knowledge will provide insights into the mechanisms by
77 which the associated risk factors for severe COVID-19 impact immune homeostasis in general.
78

79 Here we investigated early host-virus interactions to understand the mechanisms by which SARS-
80 CoV-2 induces an innate response, whether it can escape consequent innate immune control and
81 how it may propagate an immunopathogenic response. We focussed on lung epithelial cells and
82 primary macrophages, which represent cells responsible for the earliest innate immune response
83 to the virus (Bost *et al*, 2020; Chua *et al*, 2020). We found rapid replication and infectious virus
84 release in lung epithelial cells prior to potent innate immune activation. Indeed, the cocktail of
85 soluble mediators produced by infected cells strongly activated macrophages, which propagated
86 a pro-inflammatory response. Critically, the production of an inflammatory secretome was
87 directly downstream of RNA sensing by RIG-I and MDA5 because manipulation of sensing or
88 signaling events in infected cells, using RNA interference or signalling pathway inhibition,
89 suppressed subsequent macrophage activation and inflammatory gene expression. Furthermore,
90 pre-exposure of epithelial cells or macrophages to exogenous inflammatory stimuli exacerbated
91 inflammatory responses upon SARS-CoV-2 exposure. We propose that the innate immune
92 microenvironment, in which sensing of SARS-CoV-2 infection occurs, determines the degree of
93 virus-induced inflammation, and has the potential to drive disease.

94

95 **Results**

96 **SARS-CoV-2 activates delayed innate immune responses in lung epithelial cells**

97 In order to investigate innate immune responses to SARS-CoV-2, we first sought a producer cell
98 line that did not respond to the virus, thereby allowing production of virus stocks free of

99 inflammatory cytokines. As adaptive mutations have been reported during passage of the virus
100 in Vero.E6 cells (Davidson *et al*, 2020; Ogando *et al*, 2020), we selected human gastrointestinal
101 Caco-2 cells, which express the SARS-CoV-2 receptor ACE2 and entry factors TMPRSS2/4 (Figure
102 EV1A, B) and are naturally permissive (Stanifer *et al*, 2020). We found that Caco-2 support high
103 levels of viral production (Figure EV1C, D), but not virus spread (<15% cells infected) (Figure EV1E,
104 F). Importantly, they do not mount a detectable innate response to SARS-CoV-2 over 72 hpi at a
105 range of multiplicities of infection (MOIs), as evidenced by a lack of interferon stimulated gene
106 induction (ISG) (Figure EV1G). They are also broadly less responsive to innate immune agonists
107 than lung epithelial Calu-3 cells (compare Figure EV1H-Caco-2 and Figure EV1I-Calu-3). Caco-2
108 cells were therefore used to produce SARS-CoV-2 stocks uncontaminated by inflammatory
109 cytokines.

110

111 Comparatively, lung epithelial Calu-3 cells express high levels of receptor ACE2, and entry co-
112 factors TMPRSS2 and TMPRSS4 (Figure EV1A and B) (Hoffmann *et al*, 2020; Zang *et al*, 2020), and
113 are innate immune competent (Figure EV1I) when stimulated with various PRR agonists.
114 Consistently, Calu-3 cells supported very rapid spreading infection of SARS-CoV-2 followed by
115 activation of innate immune responses. SARS-CoV-2 replication displayed >1000-fold increase in
116 viral genomic and subgenomic (envelope, E) RNA levels within 5 hours post infection (hpi) across
117 a range of MOIs 0.08, 0.4, 2 TCID50/cell (Figure 1A, Figure EV2A), with TCID50 determined in
118 Vero.E6 cells. Genomic and subgenomic E RNA in Calu-3 plateaued around 10 hpi. Rapid
119 spreading infection was evidenced by increasing nucleocapsid protein (N)-positive cells by flow
120 cytometry and immunofluorescence staining, peaking at 24 hpi with 50-60% infected cells
121 (Figures 1B-D and Figure EV2B). Infectious virus was evident in supernatants by 5 hpi at the
122 highest MOI and peaked between 10-48 hpi, depending on MOI (Figure 1E, Figure EV2C). A
123 pronounced innate immune response to infection followed the peak of viral replication,
124 evidenced by induction of cytokines (IL-6, TNF), chemokines (CCL2, CCL5) and type I and III IFNs
125 (IFNβ, IFNλ1/3) measured by RT-qPCR (Figures 1F and G, and Figure EV2D-F). This was
126 accompanied by an IFN-stimulated gene (ISG) expression signature (CXCL10, IFIT1, IFIT2, MxA)
127 (Figure 1H and Figure EV2D-F). Gene induction was virus dose-dependent at 24 hpi, but equalised

128 across all MOIs by 48 hpi, as the antiviral response to low-dose virus input maximised. These data
129 show that infected lung epithelial cells can be a direct source of inflammatory mediators.

130

131 We were surprised that SARS-CoV-2 replicated so efficiently in Calu-3 despite innate immune
132 responses including IFN and ISG expression because coronaviruses, including SARS-CoV-2 are
133 reported to be IFN sensitive (Stanifer *et al.*, 2020). Indeed, recombinant Type I IFN, but not type
134 II or type III IFNs, effectively reduced SARS-CoV-2 replication if Calu-3 cells were treated prior to
135 infection (Figure 1I-K, Figure EV2G and H). However, Type I IFN had little effect on viral replication
136 when added two hours after infection (Figure 1 I-K). Thus, the IFN response induced in infected
137 lung epithelial Calu-3 cells appears too late to suppress SARS-CoV-2 replication in this system. To
138 determine if viral exposure dose influences the race between viral replication and IFN, we
139 infected cells at a 100x lower dose (MOI 0.0004 TCID50/cell) and observed a longer window of
140 opportunity for exogenous Type I IFN to restrict viral replication (Figure 1 I-K). This is consistent
141 with the hypothesis that high-dose infection can overcome IFN-inducible restriction.

142

143 **Peak SARS-CoV-2 replication precedes innate immune activation**

144 To understand the apparent disconnect in the kinetics between innate immune activation and
145 viral replication, we used single-cell imaging to measure nuclear localisation of activated
146 inflammatory transcription factors NF-κB p65 and IRF3, which mediate multiple PRR-signalling
147 cascades. NF-κB p65 nuclear translocation coincided with cells becoming N protein positive and
148 a change was evident from 5 hpi (Figure 2A and B, Figure EV3A). The timing of NF-κB p65
149 translocation was dependant on the viral dose, from 5 hpi for the highest MOI (2 TCID50/cell,
150 Figure EV3), between 5 - 10 hpi for MOIs 0.4 and 0.04 (Figures 2A and B, Figure EV3), and 24 – 48
151 hpi for MOI 0.004 (Figure EV3). IRF3 activation was also virus dose dependent but did not
152 maximise until 72 hpi, later than NF-κB (Figures 2C and D, Figure EV3), and we observed a more
153 modest shift in IRF3 nuclear intensity compared to NF-κB throughout infection. These data are
154 consistent with the requirement of a threshold of viral RNA replication to induce transcription
155 factor translocation and innate immune activation, and suggest that SARS-CoV-2 may antagonise

156 IRF3 activation to a greater extent than NF-κB. Although small variation in NF-κB p65 and IRF3
157 nuclear intensity was observed in N negative cells, we did not see the same large increases
158 sustained throughout the timecourse as in N positive cells, consistent with direct activation of
159 NF-κB p65 and IRF3 by virus replication (Figure EV3).
160
161 Supporting the observation of activation of NF-κB p65 and IRF3 activation by SARS-CoV-2
162 infection, single cell fluorescence *in situ* hybridisation (FISH) analysis of IL-6 mRNA (a prototypic
163 NF-κB regulated cytokine), showed increased IL-6 transcripts uniquely in N-positive infected cells,
164 appearing at 6 hpi and peaking at 24hpi (Figure 2E and F, Figure EV4A). IFIT1 transcripts (a
165 prototypic ISG) measured by FISH also demonstrated rapid induction in N-positive cells with
166 increased signal from at 6 hpi (Figure 2G and H). Strikingly, IFIT1 mRNA was not highly induced in
167 N-negative bystander cells consistent with defective interferon responses failing to induce ISGs
168 and a timely antiviral state in uninfected cells (Figure 2H). As a control for these changes, we
169 show that GAPDH transcripts did not change (Figure EV4B). Secretion of pro-inflammatory
170 chemokine CXCL10, and cytokine IL-6, followed gene expression and were detected from 24 hpi
171 (Figure 2I and J, Figure EV4C). Further analysis revealed increases in lactate dehydrogenase (LDH)
172 in infected cell supernatants from 48 hpi, equal across all MOIs, indicative of pro-inflammatory
173 cell death (Figure 2K, EV4D). Importantly cytokine secretion had also equalised across MOIs from
174 24 hpi (Figure 2I and J). LDH release paralleled loss of the epithelial monolayer integrity (Figure
175 1C) and cell death (Figure 2L, Figure EV4E and F) accounting for the reduction in cytokine
176 secretion at 72 hpi (Figures 2I and J).
177
178 **SARS-CoV-2 is sensed by MDA5 and RIG-I**
179 To determine the mechanism of virus sensing by innate pathways, we first confirmed that viral
180 RNA replication is required for innate immune activation. Inhibition of viral RNA replication, with
181 polymerase inhibitor Remdesivir, abrogated pro-inflammatory and ISG gene expression in a dose-
182 dependent manner (Figure 3A-D). Critically, Remdesivir was only effective if added prior to, or at
183 the time of infection, consistent with a requirement for metabolism to its active tri-
184 phosphorlyated form (Eastman *et al*, 2020) (Figures 3 E-H).

185

186 Inflammatory gene induction dependent on viral genome replication suggested that an RNA
187 sensor activates this innate response. Both genomic and subgenomic SARS-CoV-2 RNAs are
188 replicated via double stranded intermediates in the cytoplasm (Li *et al*, 2020). Accordingly, we
189 detected cytoplasmic dsRNA at 5 hpi in Calu-3 cells, preceding N positivity (Figure 3I) and by 48
190 hpi all dsRNA positive cells were N positive. Depletion of RNA sensing adaptor MAVS abolished
191 SARS-CoV-2-induced IL-6, CXCL10, IFNβ and IFIT2 gene expression (Figures 3 J-O), consistent with
192 RNA sensing being a key driver of SARS-CoV-2-induced innate immune activation. Concordantly,
193 depletion of cytoplasmic RNA sensors RIG-I or MDA-5 also reduced inflammatory gene expression
194 after infection (Figures 3J-O). This suggested sensing of multiple RNA-species given the different
195 specificities of RIG-I and MDA5 (Hornung *et al*, 2006; Kato *et al*, 2006; Rehwinkel *et al*, 2010; Wu
196 *et al*, 2013). Intriguingly, unlike RIG-I, MDA5 was not required for induction of NF-κB-sensitive
197 genes IL-6 or TNF, consistent with differences in downstream consequences of RIG-I and MDA5
198 activation (Figure 3N and O) (Brisse & Ly, 2019). Abrogating SARS-CoV-2 sensing via MDA5 and
199 MAVS depletion also reduced cell death, suggesting cell death is mediated by the host response
200 rather than direct virus-induced damage (Figure 3P). Notably, sensor depletion did not strongly
201 increase viral RNA levels (Figure 3Q), or the amount of released infectious virus (Figure 3R),
202 confirming that innate immune activation via RNA sensing did not potently inhibit viral
203 replication.

204

205 **NF-κB and JAK/STAT signalling drive innate immune responses**

206 As a complementary approach to mapping SARS-CoV-2-induced innate immune activation, and
207 to assess the potential of specific immunomodulators to impact inflammatory responses and viral
208 replication, we examined the effect of inhibiting NF-κB activation using IK-β kinase (IKK-β)
209 inhibitors TPCA-1 and PS1145. IKK-β is responsible for NF-κB p65 activation by phosphorylation
210 following PRR signalling. Induction of ISGs and IL-6 was inhibited by TPCA-1, and with slightly
211 reduced potency PS1145 (Figure 4A-C, Figure EV5A and B). Inhibiting Janus kinase (JAK) with
212 Ruxolitinib, to prevent JAK signalling downstream of the Type I IFN receptor (IFNAR), also
213 suppressed SARS-CoV-2 induced ISGs, but not NF-κB-sensitive IL-6 (Figure 4D-F and Figure EV5C).

214 Neither TPCA-1 nor Ruxolitinib treatment increased viral genome replication over a wide range
215 of MOIs (Figure 4G and H) or N positivity or virion production after single dose infection (Figure
216 EV5D-F). Importantly, NF-κB and JAK inhibition significantly reduced cell death in infected
217 cultures (Figure 4I). This is consistent with our earlier observation and with the notion that the
218 innate immune response to infection is the main driver of lung epithelial cell damage. Our data
219 thus far, show that SARS-CoV-2 infection of Calu-3 lung epithelial cells results in multi-pathway
220 activation, driving pro-inflammatory and IFN-mediated innate immune responses that are
221 inadequate or arise too late to restrict virus. Critically, they also suggest that SARS-CoV-2 induced
222 IFN and pro-inflammatory gene expression can be therapeutically uncoupled from viral
223 replication.
224
225 **Epithelial responses to SARS-CoV-2 drive macrophage activation**
226 Resident and recruited pro-inflammatory macrophages in the lungs are associated with severe
227 COVID-19 disease (Bost *et al.*, 2020; Liao *et al*, 2020; Pairo-Castineira *et al.*, 2020; Szabo *et al*,
228 2020). We therefore asked whether macrophages can support SARS-CoV-2 infection and how
229 they respond indirectly to infection, through exposure to conditioned medium from infected
230 epithelial cells. Importantly, neither primary monocyte-derived macrophages (MDM), nor PMA-
231 differentiated THP-1 cells (as an alternative macrophage model), supported SARS-CoV-2
232 replication, evidenced by lack of increase in viral RNA and by the absence of N positive cells
233 (Appendix Figure S1A-C). This is consistent with their lack of ACE2 and TMPRSS2 expression
234 (Figure EV1A, B). However, exposure of MDM to virus-containing conditioned medium from
235 infected Calu-3 cells (Figure 5A) led to significant macrophage ISG induction (Figure 5B, E, H) and
236 increased expression of macrophage-activation markers CD86 and HLA-DR (Figure 5C-D, F-G, I-J).
237 Importantly, the immune stimulatory activity of conditioned media was dependent on RNA
238 sensing and innate immune activation in infected Calu-3 cells because induction of inflammatory
239 genes and macrophage activation markers was abolished by depletion of MAVS prior to Calu-3
240 infection (Figure 5B-D) or by inhibition of NF-κB (TPCA-1) or JAK activation (Ruxolitinib) in
241 infected Calu-3 (Figure 5E-J). Note that in these experiments, MDM were exposed to equivalent
242 numbers of viral genomes from the MAVS depleted, or inhibitor treated conditioned media

243 (Appendix Figure S1D-F). To confirm that soluble mediators produced by infected Calu-3 cells
244 were key in driving MDM activation, we pre-treated MDM with either anti-IFN αβ receptor 2
245 (IFNAR2) antibody or Ruxolitinib to inhibit IFN signalling during exposure to CoM. Both
246 treatments reduced induction of ISG IFIT2 and CXCL10 in MDM. We also saw a trend towards
247 decreasing CCL5 expression but this was not significant, suggesting other pro-inflammatory
248 mediators contributing to gene induction in MDM (Figures 5K-M, Appendix Figure S1G-I).
249 Strikingly, inhibiting IFN signalling reduced the induction of MDM activation markers CD86 and
250 HLA-DR underlining the importance of IFN in these responses to the infected Calu-3 supernatant
251 (Figures 5N-O, Appendix Figure S1J-K). Together these data demonstrate that production of IFNs
252 and inflammatory mediators from infected lung epithelial cells, downstream of viral RNA sensing,
253 can propagate potent pro-inflammatory macrophage activation.
254
255 **Pre-existing immune activation exacerbates SARS-CoV-2-dependent inflammation**
256 Severe COVID-19 is associated with inflammatory co-morbidities suggesting that pre-existing
257 inflammatory states lead to inappropriate immune responses to SARS-CoV-2 and drive disease
258 (Lucas *et al*, 2020; Mehra *et al*, 2020; Williamson *et al*, 2020; Wolff *et al*, 2020; Zhang *et al.*, 2020).
259 Macrophages in particular are thought to potentiate inflammatory responses in the lungs of
260 severe COVID-19 patients (Liao *et al.*, 2020; Nicholls *et al*, 2003) and so we investigated whether
261 inflammatory stimuli might directly exacerbate macrophage responses to SARS-CoV-2 alone
262 (Figure 6A-H). In these experiments we produced virus in Caco-2 and therefore it did not contain
263 inflammatory cytokines (Figure EV1G). We detected low level innate immune activation after
264 exposure of MDM to SARS-CoV-2 alone (Figure 6B-H). However, when MDM were primed with
265 100 ng/ml LPS prior to exposure to SARS-CoV-2, we observed an enhanced response compared
266 to exposure to virus or LPS alone, evidenced by significantly increased levels of ISGs (Figure 6D
267 and E) and pro-inflammatory CCL5 (Figure 6C). Of note, LPS alone induced IL-6 and
268 inflammasome-associated IL-1β expression and secretion and this was unaffected by virus
269 exposure (Figure 6F-H). Exposure of MDM to SARS-CoV-2, prior to stimulation with LPS (Figure
270 6I-P), also enhanced macrophage inflammatory and ISG responses, but not IL-6 or IL-1β
271 expression and secretion, compared to those detected with virus or LPS alone (Figure 6J-P).

272 Importantly, LPS treatment of MDM, before or after virus challenge, did not alter SARS-CoV-2
273 permissivity of MDM, evidenced by no change in the level of detectable viral E gene in MDM
274 supernatants (Figure 6B and J). Thus, the changes in MDM gene induction by virus after LPS
275 treatment are due to differences in the MDM response to virus and not due to a difference in the
276 amount of virus genome added or induction of viral gene expression.
277
278 Finally, we modelled the lung epithelial cell response to the cytokines observed in activated
279 macrophages. We first selected IL-1β, as it was produced by LPS-treated, LPS-primed virus-
280 exposed and virus primed LPS-exposed MDM (Figure 6G and H, O and P) and has been observed
281 in severe COVID-19 patient lungs (Laing *et al*, 2020; Rodrigues *et al*, 2021). Treatment of Calu-3
282 with IL-1β during infection significantly increased induction of both ISGs and pro-inflammatory
283 cytokines, compared to their induction by virus alone (Figure 6Q-T). The exception was IL-6,
284 which was highly induced by virus even in the absence of IL-1β pre-treatment (Figure 6S). Next
285 we treated Calu-3 cells with TNF, which is also produced by LPS-treated or primed MDM
286 (Appendix Figure S2A and B) and implicated in severe COVID-19 (Chua *et al.*, 2020; Mahase,
287 2020), but found no enhancement of innate responses to SARS-CoV-2 (Appendix Figure S2C).
288 However, both IL-1β and TNF treatment increased virus-induced epithelial cell death (Figure 6U
289 and Appendix Figure S2D), without impacting viral replication (Figure 6V and Appendix Figure
290 S2E). Together, these data suggest that SARS-CoV-2 infection of lung epithelium can promote
291 immune activation of inflammatory macrophages, via secretion of cytokines, chemokines and
292 virus from infected cells, and that this can be exacerbated by a pre-existing pro-inflammatory
293 state. This is consistent with the hypothesis that chronic inflammatory states, rather than
294 enhanced viral replication, drive detrimental immune activation and/or cell death.
295
296 **Discussion**
297 We found that SARS-CoV-2 can replicate and spread effectively in lung epithelial Calu-3 cells over
298 a wide range of inoculum doses despite inducing potent IFN responses and ISG expression. We
299 propose that in the model system used here, innate immune activation occurs too late to
300 suppress replication and attribute this to the virus deploying innate immune evasion and

301 antagonism strategies early in infection. Indeed, coronaviruses replicate inside membranous
302 vesicles, thought to protect viral RNA species from cytoplasmic sensing, and have complex
303 capacity to antagonise innate immunity, including inhibition of MDA5 activation (Liu *et al*, 2020;
304 Xia *et al*, 2020) and preventing nuclear entry of inflammatory transcription factors (Banerjee *et*
305 *al*, 2020; Miorin *et al*, 2020; Park & Iwasaki, 2020; Totura & Baric, 2012; Yuen *et al*, 2020).
306 Consistent with the literature, our data indicate that SARS-CoV-2 more effectively antagonises
307 IRF3 activation and nuclear translocation than NF-κB. Indeed, it is possible that the innate
308 immune response and the secreted signals produced by infected cells are dysregulated by viral
309 manipulation, and that this imbalanced response contributes to disease particularly in the
310 context of underlying inflammatory pathology (Blanco-Melo *et al.*, 2020; Giamarellos-Bourboulis
311 *et al*, 2020; Lucas *et al.*, 2020).
312
313 We demonstrate that SARS-CoV-2 can be sensed by both RIG-I and MDA5 and that, through their
314 signalling adaptor MAVS, these sensors drive inflammatory responses in infected Calu-3 cells
315 (Figure 7). Concordantly, both RIG-I and MDA5 have been implicated in sensing the murine
316 coronavirus mouse hepatitis virus (Li *et al*, 2010; Roth-Cross *et al*, 2008) and MDA5 was recently
317 shown to sense SARS-CoV-2 and trigger IFN production (Rebendenne *et al*, 2021; Yin *et al*, 2021).
318 Likewise, activation of dsRNA sensor PKR has also been observed during SARS-CoV-2 infection of
319 other cell types (Li *et al.*, 2020). Interestingly, DNA sensing through cGAS-STING has also been
320 reported to contribute to inflammatory responses (Neufeldt *et al*, 2020), likely through sensing
321 of self-DNA or cellular damage. The eventual innate immune activation in Calu-3 cells is likely due
322 to sensing of viral RNA when it accumulates to a level that overcomes sequestration and pathway
323 inhibition by the virus, as well as to cellular stress responses to infection. Importantly, Calu-3 cells
324 pre-treated with IFN resist infection illustrating that innate responses can suppress SARS-CoV-2
325 replication if an antiviral state is induced prior to infection, particularly with a low viral exposure
326 dose.
327
328 Although SARS-CoV-2 RNA has been found associated with macrophages and monocytes from
329 infected patients (Bost *et al.*, 2020), we found that macrophages did not support SARS-CoV-2

330 replication. However, they were sensitive to conditioned media from infected Calu-3 containing
331 virus, IFNs and pro-inflammatory mediators, inducing high levels of chemokine and ISG mRNA
332 and expression of activation markers CD86 and HLA-DR upon exposure. Crucially, it is the
333 response of the Calu-3 cells to virus infection, via RNA sensing, that drives macrophage activation
334 in these experiments, evidenced by suppression of activation after either MAVS depletion or NF-
335 κB (TPCA-1) or JAK inhibition (Ruxolitinib) in the infected Calu-3 cells. We found that IFNs
336 produced by infected Calu-3 cells downstream of RNA sensing are key in driving MDM activation,
337 evidenced by supression of macrophage activation with IFNAR antibody, although we expect
338 other soluble mediators to contribute. This inflammatory role for IFN may explain how delayed
339 IFN response could contribute to pathogenicity rather than viral clearance (Park & Iwasaki, 2020).
340
341 A recent study suggested that sensing of abortive SARS-CoV-2 infection of macrophages may
342 contribute to their activation (Zheng *et al*, 2021). Our data do not rule out a role for detection of
343 abortive replication. However, they suggest that inflammatory mediators produced from
344 infected cells, perhaps with responses particularly skewed towards pro-inflammatory pathways
345 after viral manipulation, are key to macrophage activation. Notably, exposure of macrophages to
346 infected Caco2 supernatant, which contains virus but not significant levels of cytokine or IFN, did
347 not strongly activate the macrophages. Indeed, our results show that it is important to distinguish
348 between the effects of virus and the effects of cytokines in the viral prep. Here, we have achieved
349 this by using Caco2 cells to produce virus without significant inflammatory cytokines and
350 interferons and Calu3 to produce virus with a corresponding inflammatory secretome.
351
352 Importantly, inhibiting RNA sensing or pathway activation did not particularly increase viral
353 replication, consistent with our observation that, in this model at least, virus-induced innate
354 immune responses do not significantly inhibit SARS-CoV-2 replication. These observations
355 highlight the potential of immunomodulators in reducing SARS-CoV-2 driven inflammatory
356 disease. Indeed, suppression of JAK1/2 signalling with Baricitinib, in SARS-CoV-2 infected
357 macaques, significantly reduced macrophage recruitment and inflammatory signatures and
358 preliminary data support its use in COVID-19 (Bronte *et al*, 2020). These studies are consistent

359 with epithelial-driven inflammation contributing to myeloid cell infiltration and the role of
360 macrophages in exacerbating immune responses in COVID-19 (Giamarellos-Bourboulis *et al.*,
361 2020; Hoang *et al*, 2020; Liao *et al.*, 2020). Our data provide a framework for dissecting
362 immunomodulators as therapeutics and we propose that it is essential to test both
363 immunomodulators, and direct acting antivirals, in innate-immune competent cells, rather than
364 in Caco-2, Vero or other innate immune-inactive cell types, because the inevitable interactions
365 between virus replication and innate immune pathways can influence drug efficacy and potency
366 (Kim *et al*, 2019; Rasaiyaah *et al*, 2013; Sumner *et al*, 2020).
367
368 A key question is how our experiments in Calu-3 cells inform understanding of COVID-19. We
369 propose that by studying virus replication in innate immune competent permissive host cells we
370 can probe the earliest interactions between the virus and the host that underpin subsequent
371 inflammatory responses. Our data show that RNA sensing in infected Calu-3 cells creates a pro-
372 inflammatory milieu capable of activating primary macrophages. Crucially the combined profile
373 of pro-inflammatory mediators in this system mirrors that observed in COVID-19 *in vivo* (Bost *et*
374 *al.*, 2020; Laing *et al.*, 2020; Szabo *et al.*, 2020) and primary airway epithelial cells (Fiege *et al*,
375 2021). We propose that *in vivo* it is the innate immune microenvironment in which the virus-host
376 interaction occurs, and its consequent influence on immune activation, that determines disease
377 outcome. This is consistent with our demonstration that exogenous inflammatory stimuli can
378 drive a state in Calu-3 cells, and primary macrophages, that influences the response to virus,
379 exacerbating inflammation. This link, between the immediate epithelial response to infection and
380 external inflammatory signals, both amplified by macrophages, provides a plausible hypothesis
381 to explain the association of severe COVID-19 with the presence of proinflammatory
382 macrophages in broncheoalvolar lavage and patient lungs (Giamarellos-Bourboulis *et al.*, 2020;
383 Liao *et al.*, 2020; Szabo *et al.*, 2020) and inflammatory co-morbidities (Mehra *et al.*, 2020;
384 Williamson *et al.*, 2020; Wolff *et al.*, 2020), which could provide similar inflammatory stimulation.
385
386 It is remarkable how effective SARS-CoV-2 is in escaping human innate immune responses at the
387 cellular level, despite being a recent zoonosis. Very low levels of adaptive change are consistent

388 with adaptation to human replication prior to identification. Whether SARS-CoV-2 adapted in a
389 non-human species prior to human infection, or whether adaptation in humans occurred before
390 identification, remains unclear. One possibility is that coronaviruses replicate in a conserved
391 niche, with regard to innate immune evasion, and thus are particularly good at zoonosis, perhaps
392 evidenced by SARS-CoV-2 being preceded by SARS-CoV-1 and Middle Eastern Respiratory
393 Syndrome virus (MERS), and apparent cross species transfer and transmission in distantly related
394 species including humans, bats (Boni *et al*, 2020), camels (Azhar *et al*, 2014), civet cats (Wang &
395 Eaton, 2007) and mink (Koopmans, 2020).
396
397 Viral disease is often driven by host immune mechanisms that have evolved to protect the host
398 from death, a paradox that is particularly evident in COVID-19. Here we have taken a significant
399 step towards explaining the consequences of SARS-CoV-2 infection of innate immune competent
400 lung epithelial cells by illustrating how RNA sensing can directly drive potent inflammatory
401 responses, irrespective of whether virus replication is suppressed. We propose that further
402 studies addressing mechanisms of SARS-CoV-2 immune evasion and cytopathology, and the
403 wider impact these have on epithelial-immune cell cross-talk, will inform development of
404 effective therapeutics that are broadly active against zoonotic coronaviruses.
405

406 **Materials and Methods**

407 **Cell culture and innate immune stimulation**

408 Calu-3 cells (ATCC HTB-55) and Caco-2 cells were a kind gift Dr Dalan Bailey (Pirbright Institute)
409 and were originally obtained from ATCC. THP-1 Dual cells were obtained from Invivogen. Vero.E6
410 were provided by NIBSC, Beas2B (ATCC CRL-9609) and Hulec5a (ATCC CRL-3244) were obtained
411 from ATCC, and Detroit 562 (ATCC CCL-138) were a kind gift from Dr Caroline Weight (UCL). All
412 cells tested negative for mycoplasma by commercial assay. All cells except THP-1 were cultured
413 in Dulbecco's modified Eagle Medium (DMEM) supplemented with 10% heat-inactivated FBS
414 (Labtech), 100U/ml penicillin/streptomycin, with the addition of 1% Sodium Pyruvate (Gibco) and
415 1% Glutamax for Calu-3 and Caco-2 cells. All cells were passaged at 80% confluence. For
416 infections, adherent cells were trypsinised, washed once in fresh medium and passed through a

417 70 µm cell strainer before seeding at 0.2x10^6 cells/ml into tissue-culture plates. Calu-3 cells
418 were grown to 60-80% confluence prior to infection. THP-1 cells were cultured in RPMI (Gibco)
419 supplemented with 10 % heat-inactivated FBS (Labtech), 100U/ml penicillin/streptomycin
420 (Gibco), 25 mM HEPES (Sigma), 10 µg/ml of blasticidin (Invivogen) and 100 µg/ml of Zeocin™
421 (Invivogen). Caco-2 and Calu-3 cells were stimulated for 24 h with media containing TLR4 agonist
422 Lipopolysaccharide (LPS) (Peprotech), the TLR3 agonist poly I:C (Peprotech) or the TLR7 agonist
423 R837 (Invivogen), using the concentration stated on each figure. To stimulate RIG-I/MDA5
424 activation in Calu-3 cells, poly I:C was transfected. Transfection mixes were prepared using
425 lipofectamine 2000 (Invitrogen) in Optimem (Thermofisher Scientific) according to the
426 manufacturer's instructions.
427
428 **Isolation of primary monocyte-derived macrophages**

429 Primary monocyte-derived macrophages (MDM) were prepared from fresh blood from healthy
430 volunteers. The study was approved by the joint University College London/University College
431 London Hospitals NHS Trust Human Research Ethics Committee and written informed consent
432 was obtained from all participants. Experiments conformed to the principals set out in WMA
433 declaration of Helsinki and the Department of Health and Human Services Belmont Report.
434 Peripheral blood mononuclear cells (PBMCs) were isolated by density gradient centrifugation
435 using Lymphoprep (Stemcell Technologies). PBMCs were washed three times with PBS and plated
436 to select for adherent cells. Non-adherent cells were washed away after 2 h and the remaining
437 cells incubated in RPMI (Gibco) supplemented with 10 % heat-inactivated pooled human serum
438 (Sigma) and 100 ng/ml macrophage colony stimulating factor (Peprotech). The medium was
439 replaced after 3 days with RPMI with 5% FCS, removing any remaining non-adherent cells. Cells
440 were infected or treated with conditioned media 3-4 days later.

441 **Virus culture and infection**

442 SARS-CoV-2 strain BetaCoV/Australia/VIC01/2020 (NIBSC) was propagated by infecting Caco-2
443 cells at MOI 0.01 TCID50/cell, in DMEM supplemented with 2% FBS at 37°C. Virus was harvested
444 at 72 hours post infection (hpi) and clarified by centrifugation at 4000 rpm for 15 min at 4 °C to

445 remove any cellular debris. Virus stocks were aliquoted and stored at -80 °C. Virus titres were
446 determined by 50% tissue culture infectious dose (TCID50) on Vero.E6 cells. In brief, 96 well
447 plates were seeded at 1x10^4 cells/well in 100 µl. Eight ten-fold serial dilutions of each virus stock
448 or supernatant were prepared and 50 µl added to 4 replicate wells. Cytopathic effect (CPE) was
449 scored at 5 days post infection, and TCID50/ml was calculated using the Reed & Muench method
450 (Reed, 1938), and an Excel spreadsheet created by Dr. Brett D. Lindenbach was used for
451 calculating TCID50/mL values (Lindenbach, 2009).
452
453 For infections, multiplicities of infection (MOI) were calculated using TCID50/cell determining on
454 Vero.E6 cells. Cells were inoculated with diluted virus stocks for 2h at 37 °C. Cells were
455 subsequently washed twice with PBS and fresh culture medium was added. At indicated time
456 points, cells were harvested for analysis.
457
458 MDM were infected with virus diluted in RPMI, 5% FBS (estimated MOI 0.02 TCID50/cell). MDM
459 were harvested at 24h or 48 hpi for gene expression analysis. For priming experiments, MDM
460 were stimulated with 100 ng/mL of LPS (HC4046, Hycult Biotech) for 2h. Media was replaced and
461 cells were exposed to SARS-CoV-2 as before, diluted in RPMI, 5% FBS. Cells were collected after
462 48h for analysis. Alternatively, cells were mock exposed or exposed to SARS-CoV-2 for 3 days and
463 then stimulated with 100 ng/mL of LPS. Cells were harvested after 24h for analysis.
464
465 In macrophage experiments, a minimum sample size of six independent experiments using cells
466 derived from separate donors was used to give 90% power in order for a two-sided test to detect
467 >two-fold differences between two groups with an estimated standard deviation of 0.5.
468
469 **Sensor and adaptor depletion by RNAi**
470 Calu-3 cells were transfected with 40 pmol of siRNA SMART pool against RIG-I (L-012511-00-
471 0005), MDA5 (L-013041-00-0005), MAVS (L-024237-00-0005) or non-targeting control (D-
472 001810-10-05) (Dharmacon) using Lipofectamine *RNAiMAX* Transfection Reagent (Invitrogen).
473 Transfection medium was replaced after 24h with DMEM medium supplemented with 10% FBS,

474 100U/ml penicillin/streptomycin and cells cultured for additional 2 days. On day 3, cells were
475 transfected again with the same siRNA smart pools. Transfection medium was replaced after 24h
476 and cells cultured for additional 2 days before infection. Gene depletion was verified using
477 TaqMan Gene Expression Assay according to manufacturer's instructions detecting human RIG-I
478 (FAM dye-labelled, TaqMan probe ID no. Hs01061436_m1), MAVS (FAM dye-labelled, TaqMan
479 probe ID no. Hs00920075_m1), MDA5 (FAM dye-labelled, TaqMan probe ID no.
480 Hs00223420_m1) or the housekeeping gene OAZ1 (FAM dye-labelled, TaqMan probe ID no.
481 Hs00427923_m1)
482
483 **Treatment with cytokines, inhibitors and conditioned medium**
484 Calu-3 cells were pre-treated with Remdesivir (Selleck Chemicals), TPCA-1 (Biotechne), PS-1145
485 (BioTechne) or Ruxolitinib (Biotechne) at the indicated concentrations or DMSO control at an
486 equivalent dilution for 1 h before SARS-CoV-2 infection unless otherwise stated. Inhibitors were
487 maintained at the indicated concentrations throughout the experiments. For cytokine
488 treatments, recombinant human IFNβ, IFNλ1, IFNλ2, IFNγ, IL1β or TNF (Peprotech) at a final
489 concentration of 10 ng/ml were added at the indicated time points. To generate conditioned
490 media (CoM), Calu-3 cells were mock-infected or infected with SARS-CoV-2 at 0.04 TCID50/cell
491 and supernatants were harvested 48 hpi, clarified by centrifugation at 4000 rpm for 15 minutes
492 and 4 °C and stored at -80 °C. For conditioned media experiments, MDM were exposed to CoM
493 as indicated, which was diluted 1:5 in RPMI, 5% FBS. After 6 hours, conditioned medium was
494 replaced with RPMI, 5% FBS and cells were harvested at 48 h for gene expression and surface
495 marker expression analysis. MDM were treated where indicated during CoM exposure with
496 either 2 μM ruxolitinib (Biotechne) or 2.5 μg/ml anti-IFNAR antibody (pbl Assay Science) or an
497 isotype control IgG2A antibody (R&D).
498
499 **RT-qPCR**
500 RNA was extracted using RNeasy Micro Kits (Qiagen) and residual genomic DNA was removed
501 from RNA samples by on-column DNAse I treatment (Qiagen). Both steps were performed
502 according to the manufacturer's instructions. cDNA was synthesized using SuperScript III with

503 random hexamer primers (Invitrogen). RT-qPCR was performed using Fast SYBR Green Master
504 Mix (Thermo Fisher) for host gene expression or TaqMan Master mix (Thermo Fisher) for viral
505 RNA quantification, and reactions performed on the QuantStudio 5 Real-Time PCR systems
506 (Thermo Fisher). Host gene expression was determined using the 2-ΔΔCt method and normalised
507 to GAPDH expression. Viral RNA copies were deduced by standard curve, using primers and a
508 Taqman probe specific for E, as described elsewhere (Corman *et al*, 2020) and below.
509 The following primers and probes were used:

Target	Sequence
ACE2	Fwd 5'-CGAAGCCGAAGACCTGTTCTA -3' Rev 5'-GGGCAAGTGTGGACTGTTC-3'
CCL5	Fwd: 5'-CCCAGCAGTCGTCTTTGTCA-3' Rev 5'- TCCCGAACCCATTTCTTCTCT-3'
CXCL10	Fwd 5'-TGGCATTCAAGGAGTACCTC-3' Rev 5'-TTGTAGCAATGATCTCAACACG-3'
GAPDH	Fwd 5'-GGGAAACTGTGGCGTGAT-3' Rev 5'-GGAGGAGTGGGTGTCGCTGTT-3'
IFIT1	Fwd 5'-CCTCCTTGGGTTCGTCTACA-3' Rev 5'-GGCTGATATCTGGGTGCCTA-3'
IFIT2	Fwd 5'-CAGCTGAGAATTGCACTGCAA-3' Rev 5'-CGTAGGCTGCTCTCCAAGGA-3'
IFNB1	Fwd 5'-AGGACAGGATGAACTTTGAC-3' Rev 5'-TGATAGACATTAGCCAGGAG-3'
IFNL1	Fwd 5'-CACATTGGCAGGTTCAAATCTCT-3' Rev 5'- CCAGCGGACTCCTTTTTGG-3'
IFNL3	Fwd 5'- TAAGAGGGCCAAAGATGCCTT-3' Rev 5'- CTGGTCCAAGACATCCCCC-3'
IL1B	Fwd: 5'- CCTCCTTGGGTTCGTCTACA-3' Rev 5'-GGCTGATATCTGGGTGCCTA-3'
IL6	Fwd 5'-AAATTCGGTACATCCTCGACG-3' Rev 5'-GGAAGGTTCAGGTTGTTTTCT-3'
MX1	Fwd 5'-ATCCTGGGATTTTGGGGCTT-3' Rev 5'-CCGCTTGTCGCTGGTGTCG-3'
TMPRSS2	Fwd 5'-CAAGTGCTCCAACTCTGGGAT -3' Rev 5'-AACACACCGATTCTCGTCCTC-3'
TMPRSS4	Fwd 5'-ATGCGGAACTCAAGTGGGC-3' Rev 5'-CTGTTTGTCGTACTGGATGCT-3'

TNF	Fwd 5'-AGCCTCTTCTCCTTCCTGATCGTG-3' Rev 5'-GGCTGATTAGAGAGAGGTCCCTGG-3'
SARS-CoV-2 E_Sarbeco_F	5'-ACAGGTACGTTAATAGTTAATAGCGT-3'
SARS-CoV-2 E_Sarbeco_Probe1	5'-FAM-ACACTAGCCATCCTTACTGCGCTTCG-TAMRA-3'
SARS-CoV-2 E_Sarbeco_R	5'-ATATTGCAGCAGTACGCACACA-3'

510

511 **Cytokine and LDH measurement**

512 Secreted mediators were detected in cell culture supernatants by ELISA. CXCL10 and IL6 protein
513 were measured using Duoset ELISA reagents (R&D Biosystems) according to the manufacturer's
514 instructions.

515 Secreted lactate dehydrogenase (LDH) activity was measured as a correlate of cell death in
516 culture supernatants using Cytotoxicity Detection Kit^{PLUS} (Sigma) according to the manufacturer's
517 instructions. Culture supernatants were collected at the indicated time points post infection,
518 clarified by centrifugation and stored at 4 °C until LDH measurement.

519

520 **Antibodies**

521 All antibody sources are cited with sample identifiers and all antibodies were validated for their
522 specific use by manufacturers or by previously published work as cited.

523

524 **Flowcytometry**

525 For flowcytometry analysis, adherent cells were recovered by trypsinising or gentle scraping and
526 washed in PBS with 2mM EDTA (PBS/EDTA). Non-adherent cells were recovered from culture
527 supernatants by centrifugation for 5 min at 1600 rpm and washed once in PBS/EDTA. Cells were
528 stained with fixable Zombie UV Live/Dead dye (Biolegend) for 6 min at room temperature. Excess
529 stain was quenched with FBS-complemented DMEM. For MDMs, Fc-blocking was performed with
530 PBS/EDTA+10% human serum for 10 min at 4˚C. Cell surface with CD86-Bv711 (IT2.2, Biolegend)
531 and HLA-DR-PerCpCy5.5 or PE-Cy7 (L243, Biolegend) staining was performed in PBS/EDTA at 4˚C
532 for 30min. Unbound antibody was washed off thoroughly and cells were fixed in 4% PFA prior to

533 intracellular staining. For intracellular detection of SARS-CoV-2 nucleoprotein, cells were
534 permeabilised for 15 min with Intracellular Staining Perm Wash Buffer (BioLegend). Cells were
535 then incubated with 1µg/ml CR3009 SARS-CoV-2 cross-reactive antibody (a kind gift from Dr.
536 Laura McCoy) in permeabilisation buffer for 30 min at room temperature, washed once and
537 incubated with secondary Alexa Fluor 488-Donkey-anti-Human IgG (Jackson Labs). All samples
538 were acquired on a BD Fortessa X20 or LSR II using BD FACSDiva software. Data was analysed
539 using FlowJo v10 (Tree Star).
540
541 **Western blotting**
542 For detection of ACE2 expression, whole cell protein lysates were separated by SDS-PAGE,
543 transferred onto nitrocellulose and blocked in PBS with 0.05% Tween 20 and 5% skimmed milk.
544 Membranes were probed with polyclonal goat anti-human ACE2 (1:500, AF933, R&D Biosystems)
545 or rabbit anti-human beat-Actin (1:2500, 6L12, Sigma) followed by donkey anti-goat IRdye
546 680CW or goat anti-rabbit IRdye 800CW (Abcam), respectively. Blots were Imaged using an
547 Odyssey Infrared Imager (LI-COR Biosciences) and analysed with Image Studio Lite software.
548
549 **Immunofluorescence microscopy and RNA-fluorescent *in situ* hybridization**
550 For imaging analysis, Calu-3 or Caco-2 cells were seeded and infected with SARS-CoV-2 in Optical
551 96-well plates (CellCarrier Ultra, PerkinElmer) and cells were fixed with 4% PFA at the indicated
552 timepoints. Permeabilisation was carried out with 0.1% TRITON-X100 (Sigma) in PBS for 15
553 minutes. A blocking step was carried out for 1h at room temperature with 10% goat
554 serum/1%BSA in PBS. Nucleocapsid (N) proten detection was performed by primary incubation
555 with human anti-N antibody (Cr3009, 1ug/ml) for 18h, and washed thoroughly in PBS. Where
556 appropriate, N-protein staining was followed by incubation with rabbit anti-NF-κB (p65) (sc-372,
557 Santa Cruz) or rabbit anti-IRF3 (sc-9082, Santa Cruz) for 1 h. Primary antibodies were detected by
558 labelling with with secondary anti-human AlexaFluor488 and anti-rabbit AlexaFluor546
559 conjugates (Jackson Immuno Research) for 1h. For RNA fluorescent *in situ* hybridization **(**FISH),
560 cells were immunofluorescently labelled for viral N-protein (detected with AlexaFluor488 or
561 AlexaFluor546 conjugates) followed by RNA visualisation using the ViewRNA Cell Plus Kit (Thermo

562 Fisher). The ViewRNA probes implemented targeted *IL-6* (VA4-19075, AlexaFluor488), *IFIT1* (VA4-
563 18833, AlexaFluor488) and *GAPDH* (VA1-10119, AlexaFluor546). All cells were then labelled with
564 HCS CellMask DeepRed (H32721, Thermo Fisher) and Hoechst33342 (H3570, Thermo Fisher).
565 Images were acquired using the WiScan® Hermes High-Content Imaging System (IDEA Bio-
566 medical, Rehovot, Israel) at magnification 10X/0.4NA or 40X/0.75NA. Four channel automated
567 acquisition was carried out sequentially (DAPI/TRITC, GFP/Cy5). For 10X magnification 100%
568 density/100% well area was acquired, resulting in 64 FOV/well. For 40X magnification, 35%
569 density/ 30% well area was acquired resulting in 102 FOV/well.
570
571 **Image analysis**
572 NF-κB, IRF3, *IL6* and *GAPDH* raw image channels were pre-processed using a batch rolling ball
573 background correction in FIJI imagej software package (Schindelin *et al*, 2012) prior to
574 quantification. Automated image analysis was carried out using the 'Athena' HCS analysis
575 software package (IDEA Bio-medical IDEA Bio-medical, Rehovot, Israel). For quantification of the
576 percentage of nucleocapsid positive cells within the population, the 'Intracellular Granules'
577 module was utilised. Nuclei were segmented using Hoechst33342 signal. Cell boundaries were
578 determined by segmentation of CellMask signal. Infected cells were determined by thresholding
579 intracellular N protein signal (Intracellular granules). For all analysis, the N protein signal intensity
580 was thresholded against the mock infected wells to ensure no false segmentation of N +ve
581 objects. Nuclear accumulation of NF-κB or IRF3 was carried out using the 'Intranuclear Foci'
582 module. Nuclei of cells were segmented using the Hoechst33342 stain. 'Foci' of perinuclear N
583 protein signal were identified and an 'Infected' cell population determined based on the presence
584 of such segmented foci objects. In all cells the NF-κB or IRF3 signal present within segmented
585 nuclei was quantified. For RNA-FISH quantification the 'Mitochondria' module was implemented.
586 Nuclei were segmented using the Hoechst33342 stain. Cell cytoplasmic area was determined by
587 segmentation of CellMask 647 signal. Intracellular N protein signal was segmented as
588 'mitochondria' objects. *IL-6*/*GAPDH* RNA FISH signal within segmented cells was then quantified.
589 Infected cells were determined by the presence of N protein segmented objects within the cell.
590 Analysis parameters are detailed in Appendix Tables S1-7.

591

592 **Statistical analysis**

593 Statistical analysis was performed using GraphPad Prism. As indicated, normally distributed data
594 was analysed for statistical significance by *t*- tests (when comparing two groups) or one-way
595 ANOVA with Bonferroni or Dunnett's post-test (when comparing more than two groups).
596 Wilcoxon ranked paired non-parametric tests were performed for primary macrophage data that
597 was not normally distributed. For imaging analysis, where appropriate, integrated intensities
598 were normalised to the mean intensity of the mock infected population for that respective
599 timepoint. Comparisons were made using a Kruskal-Wallis test with Dunn's multiple comparison.
600 Data show the mean +/- the S.E.M, where appropriate the median is shown, with significance
601 shown on the figures, levels were defined as *, $P < 0.05$; **, $P < 0.01$ and ***, $P < 0.001$, ****, P
602 < 0.0001.

603

604 **Author Contributions**

605 Conceptualisation: LGT, AR, LZA, CJ, GJT; Experimental set up, investigation and analysis: LGT,
606 AR, LZA, MVXW, JT, MN, GJT; Writing, review and editing: all authors.

607

608 **Data Availability Section**

609 This study includes no data deposited in external repositories.
610

611 **Conflict of Interest Statement**

612 The authors have no conflicts of interest to declare.
613

614 **Acknowledgements**

615 MN (207511)and CJ (108079) are funded by Wellcome Investigator Awards, and GJT was funded
616 by a Wellcome Senior Fellowship (108183) followed by a Wellcome Investigator Award (220863).
617 MVXW is supported by the NIHR Biomedical Research Centre at UCLH and IDEA Bio-Medical Ltd.
618 Funds were also obtained from the University College London COVID-19 fund and the National
619 Institutes of Health Research UCL/UCLH Biomedical Research Centre. We are grateful to Giada
620 Mattiuzzo at NIBSC for SARS-CoV-2 and reagents, Laura McCoy at UCL for SARS-CoV-2 N antibody,
621 Dalan Bailey at The Pirbright Institute for cell lines and Richard Milne at UCL for valuable
622 discussions and critical reading of the manuscript.
623

624

625

626 **References**

627 Allen WE, Altae-Tran H, Briggs J, Jin X, McGee G, Shi A, Raghavan R, Kamariza M, Nova N, Pereta
628 A *et al* (2020) Population-scale longitudinal mapping of COVID-19 symptoms, behaviour and
629 testing. *Nature human behaviour* 4: 972-982
630 Azhar EI, El-Kafrawy SA, Farraj SA, Hassan AM, Al-Saeed MS, Hashem AM, Madani TA (2014)
631 Evidence for camel-to-human transmission of MERS coronavirus. *The New England journal of*
632 *medicine* 370: 2499-2505
633 Banerjee AK, Blanco MR, Bruce EA, Honson DD, Chen LM, Chow A, Bhat P, Ollikainen N,
634 Quinodoz SA, Loney C *et al* (2020) SARS-CoV-2 Disrupts Splicing, Translation, and Protein
635 Trafficking to Suppress Host Defenses. *Cell* 183: 1325-1339.e1321
636 Bastard P, Rosen LB, Zhang Q, Michailidis E, Hoffmann HH, Zhang Y, Dorgham K, Philippot Q,
637 Rosain J, Béziat V *et al* (2020) Autoantibodies against type I IFNs in patients with life-
638 threatening COVID-19. *Science (New York, NY)* 370
639 Beigel JH, Tomashek KM, Dodd LE, Mehta AK, Zingman BS, Kalil AC, Hohmann E, Chu HY,
640 Luetkemeyer A, Kline S *et al* (2020) Remdesivir for the Treatment of Covid-19 — Final Report.
641 *New England Journal of Medicine* 383: 1813-1826
642 Blanco-Melo D, Nilsson-Payant BE, Liu WC, Uhl S, Hoagland D, Møller R, Jordan TX, Oishi K,
643 Panis M, Sachs D *et al* (2020) Imbalanced Host Response to SARS-CoV-2 Drives Development of
644 COVID-19. *Cell* 181: 1036-1045.e1039
645 Boni MF, Lemey P, Jiang X, Lam TT, Perry BW, Castoe TA, Rambaut A, Robertson DL (2020)
646 Evolutionary origins of the SARS-CoV-2 sarbecovirus lineage responsible for the COVID-19
647 pandemic. *Nature microbiology* 5: 1408-1417
648 Bost P, Giladi A, Liu Y, Bendjelal Y, Xu G, David E, Blecher-Gonen R, Cohen M, Medaglia C, Li H *et*
649 *al* (2020) Host-Viral Infection Maps Reveal Signatures of Severe COVID-19 Patients. *Cell* 181:
650 1475-1488.e1412
651 Brisse M, Ly H (2019) Comparative Structure and Function Analysis of the RIG-I-Like Receptors:
652 RIG-I and MDA5. *Frontiers in Immunology* 10
653 Bronte V, Ugel S, Tinazzi E, Vella A, De Sanctis F, Canè S, Batani V, Trovato R, Fiore A, Petrova V
654 *et al* (2020) Baricitinib restrains the immune dysregulation in patients with severe COVID-19. *J*
655 *Clin Invest* 130: 6409-6416
656 Chua RL, Lukassen S, Trump S, Hennig BP, Wendisch D, Pott F, Debnath O, Thürmann L, Kurth F,
657 Völker MT *et al* (2020) COVID-19 severity correlates with airway epithelium-immune cell
658 interactions identified by single-cell analysis. *Nature biotechnology* 38: 970-979
659 Corman VM, Landt O, Kaiser M, Molenkamp R, Meijer A, Chu DK, Bleicker T, Brünink S,
660 Schneider J, Schmidt ML *et al* (2020) Detection of 2019 novel coronavirus (2019-nCoV) by real-
661 time RT-PCR. *Euro Surveill* 25: 2000045
662 Davidson AD, Williamson MK, Lewis S, Shoemark D, Carroll MW, Heesom KJ, Zambon M, Ellis J,
663 Lewis PA, Hiscox JA *et al* (2020) Characterisation of the transcriptome and proteome of SARS-
664 CoV-2 reveals a cell passage induced in-frame deletion of the furin-like cleavage site from the
665 spike glycoprotein. *Genome medicine* 12: 68

666 Docherty AB, Harrison EM, Green CA, Hardwick HE, Pius R, Norman L, Holden KA, Read JM,
667 Dondelinger F, Carson G *et al* (2020) Features of 20 133 UK patients in hospital with covid-19
668 using the ISARIC WHO Clinical Characterisation Protocol: prospective observational cohort
669 study. *BMJ (Clinical research ed)* 369: m1985
670 Eastman RT, Roth JS, Brimacombe KR, Simeonov A, Shen M, Patnaik S, Hall MD (2020)
671 Remdesivir: A Review of Its Discovery and Development Leading to Emergency Use
672 Authorization for Treatment of COVID-19. *ACS central science* 6: 672-683
673 Fiege JK, Thiede JM, Nanda HA, Matchett WE, Moore PJ, Montanari NR, Thielen BK, Daniel J,
674 Stanley E, Hunter RC *et al* (2021) Single cell resolution of SARS-CoV-2 tropism, antiviral
675 responses, and susceptibility to therapies in primary human airway epithelium. *PLoS Pathog* 17:
676 e1009292
677 Giamarellos-Bourboulis EJ, Netea MG, Rovina N, Akinosoglou K, Antoniadou A, Antonakos N,
678 Damoraki G, Gkavogianni T, Adami ME, Katsaounou P *et al* (2020) Complex Immune
679 Dysregulation in COVID-19 Patients with Severe Respiratory Failure. *Cell host & microbe* 27:
680 992-1000.e1003
681 Hoang TN, Pino M, Boddapati AK, Viox EG, Starke CE, Upadhyay AA, Gumber S, Nekorchuk M,
682 Busman-Sahay K, Strongin Z *et al* (2020) Baricitinib treatment resolves lower-airway
683 macrophage inflammation and neutrophil recruitment in SARS-CoV-2-infected rhesus
684 macaques. *Cell*
685 Hoffmann M, Kleine-Weber H, Schroeder S, Krüger N, Herrler T, Erichsen S, Schiergens TS,
686 Herrler G, Wu NH, Nitsche A *et al* (2020) SARS-CoV-2 Cell Entry Depends on ACE2 and TMPRSS2
687 and Is Blocked by a Clinically Proven Protease Inhibitor. *Cell* 181: 271-280.e278
688 Hornung V, Ellegast J, Kim S, Brzózka K, Jung A, Kato H, Poeck H, Akira S, Conzelmann KK, Schlee
689 M *et al* (2006) 5'-Triphosphate RNA is the ligand for RIG-I. *Science (New York, NY)* 314: 994-997
690 Kato H, Takeuchi O, Sato S, Yoneyama M, Yamamoto M, Matsui K, Uematsu S, Jung A, Kawai T,
691 Ishii KJ *et al* (2006) Differential roles of MDA5 and RIG-I helicases in the recognition of RNA
692 viruses. *Nature* 441: 101-105
693 Kim K, Dauphin A, Komurlu S, McCauley SM, Yurkovetskiy L, Carbone C, Diehl WE, Strambio-De-
694 Castillia C, Campbell EM, Luban J (2019) Cyclophilin A protects HIV-1 from restriction by human
695 TRIM5α. *Nature microbiology* 4: 2044-2051
696 Koopmans M (2020) SARS-CoV-2 and the human-animal interface: outbreaks on mink farms.
697 *The Lancet Infectious diseases*
698 Laing AG, Lorenc A, Del Molino Del Barrio I, Das A, Fish M, Monin L, Muñoz-Ruiz M, McKenzie
699 DR, Hayday TS, Francos-Quijorna I *et al* (2020) A dynamic COVID-19 immune signature includes
700 associations with poor prognosis. *Nature medicine* 26: 1623-1635
701 Li J, Liu Y, Zhang X (2010) Murine coronavirus induces type I interferon in oligodendrocytes
702 through recognition by RIG-I and MDA5. *Journal of virology* 84: 6472-6482
703 Li Y, Renner DM, Comar CE, Whelan JN, Reyes HM, Cardenas-Diaz FL, Truitt R, Tan LH, Dong B,
704 Alysandratos KD *et al* (2020) SARS-CoV-2 induces double-stranded RNA-mediated innate
705 immune responses in respiratory epithelial derived cells and cardiomyocytes. *bioRxiv : the*
706 *preprint server for biology*
707 Liao M, Liu Y, Yuan J, Wen Y, Xu G, Zhao J, Cheng L, Li J, Wang X, Wang F *et al* (2020) Single-cell
708 landscape of bronchoalveolar immune cells in patients with COVID-19. *Nature medicine* 26:
709 842-844

710 Lindenbach BD (2009) Measuring HCV infectivity produced in cell culture and in vivo. *Methods*
711 *in molecular biology (Clifton, NJ)* 510: 329-336
712 Liu G, Lee JH, Parker ZM, Acharya D, Chiang JJ, van Gent M, Riedl W, Davis-Gardner ME, Wies E,
713 Chiang C *et al* (2020) ISG15-dependent Activation of the RNA Sensor MDA5 and its Antagonism
714 by the SARS-CoV-2 papain-like protease. *bioRxiv : the preprint server for biology*
715 Lucas C, Wong P, Klein J, Castro TBR, Silva J, Sundaram M, Ellingson MK, Mao T, Oh JE, Israelow
716 B *et al* (2020) Longitudinal analyses reveal immunological misfiring in severe COVID-19. *Nature*
717 584: 463-469
718 Mahase E (2020) Covid-19: Anti-TNF drug adalimumab to be trialled for patients in the
719 community. *BMJ (Clinical research ed)* 371: m3847
720 Mehra MR, Desai SS, Kuy S, Henry TD, Patel AN (2020) Cardiovascular Disease, Drug Therapy,
721 and Mortality in Covid-19. *New England Journal of Medicine* 382: e102
722 Miorin L, Kehrer T, Sanchez-Aparicio MT, Zhang K, Cohen P, Patel RS, Cupic A, Makio T, Mei M,
723 Moreno E *et al* (2020) SARS-CoV-2 Orf6 hijacks Nup98 to block STAT nuclear import and
724 antagonize interferon signaling. *Proceedings of the National Academy of Sciences of the United*
725 *States of America* 117: 28344-28354
726 Neufeldt CJ, Cerikan B, Cortese M, Frankish J, Lee J-Y, Plociennikowska A, Heigwer F, Joecks S,
727 Burkart SS, Zander DY *et al* (2020) SARS-CoV-2 infection induces a pro-inflammatory cytokine
728 response through cGAS-STING and NF-κB. *bioRxiv : the preprint server for biology*:
729 2020.2007.2021.212639
730 Nicholls JM, Poon LL, Lee KC, Ng WF, Lai ST, Leung CY, Chu CM, Hui PK, Mak KL, Lim W *et al*
731 (2003) Lung pathology of fatal severe acute respiratory syndrome. *Lancet (London, England)*
732 361: 1773-1778
733 Ogando NS, Dalebout TJ, Zevenhoven-Dobbe JC, Limpens R, van der Meer Y, Caly L, Druce J, de
734 Vries JJC, Kikkert M, Bárcena M *et al* (2020) SARS-coronavirus-2 replication in Vero E6 cells:
735 replication kinetics, rapid adaptation and cytopathology. *The Journal of general virology* 101:
736 925-940
737 Pairo-Castineira E, Clohisey S, Klaric L, Bretherick AD, Rawlik K, Pasko D, Walker S, Parkinson N,
738 Fourman MH, Russell CD *et al* (2020) Genetic mechanisms of critical illness in Covid-19. *Nature*
739 Paranjpe I, Russak AJ, De Freitas JK, Lala A, Miotto R, Vaid A, Johnson KW, Danieletto M, Golden
740 E, Meyer D *et al* (2020) Retrospective cohort study of clinical characteristics of 2199
741 hospitalised patients with COVID-19 in New York City. *BMJ open* 10: e040736
742 Park A, Iwasaki A (2020) Type I and Type III Interferons - Induction, Signaling, Evasion, and
743 Application to Combat COVID-19. *Cell host & microbe* 27: 870-878
744 Rasaiyaah J, Tan CP, Fletcher AJ, Price AJ, Blondeau C, Hilditch L, Jacques DA, Selwood DL, James
745 LC, Noursadeghi M *et al* (2013) HIV-1 evades innate immune recognition through specific
746 cofactor recruitment. *Nature* 503: 402-405
747 Rebendenne A, Valadão ALC, Tauziet M, Maarifi G, Bonaventure B, McKellar J, Planès R, Nisole
748 S, Arnaud-Arnould M, Moncorgé O *et al* (2021) SARS-CoV-2 triggers an MDA-5-dependent
749 interferon response which is unable to control replication in lung epithelial cells. *Journal of*
750 *virology*
751 Reed LJM, H (1938) A simple method of estimating fifty percent end points. *Am J Hyg* 27: 493-
752 497

753 Rehwinkel J, Tan CP, Goubau D, Schulz O, Pichlmair A, Bier K, Robb N, Vreede F, Barclay W,
754 Fodor E *et al* (2010) RIG-I detects viral genomic RNA during negative-strand RNA virus infection.
755 *Cell* 140: 397-408
756 Rodrigues TS, de Sá KSG, Ishimoto AY, Becerra A, Oliveira S, Almeida L, Gonçalves AV, Perucello
757 DB, Andrade WA, Castro R *et al* (2021) Inflammasomes are activated in response to SARS-CoV-2
758 infection and are associated with COVID-19 severity in patients. *The Journal of experimental*
759 *medicine* 218
760 Roth-Cross JK, Bender SJ, Weiss SR (2008) Murine coronavirus mouse hepatitis virus is
761 recognized by MDA5 and induces type I interferon in brain macrophages/microglia. *Journal of*
762 *virology* 82: 9829-9838
763 Schindelin J, Arganda-Carreras I, Frise E, Kaynig V, Longair M, Pietzsch T, Preibisch S, Rueden C,
764 Saalfeld S, Schmid B *et al* (2012) Fiji: an open-source platform for biological-image analysis.
765 *Nature methods* 9: 676-682
766 Stanifer ML, Kee C, Cortese M, Zumaran CM, Triana S, Mukenhirn M, Kraeusslich HG,
767 Alexandrov T, Bartenschlager R, Boulant S (2020) Critical Role of Type III Interferon in
768 Controlling SARS-CoV-2 Infection in Human Intestinal Epithelial Cells. *Cell reports* 32: 107863
769 Sumner RP, Harrison L, Touizer E, Peacock TP, Spencer M, Zuliani-Alvarez L, Towers GJ (2020)
770 Disrupting HIV-1 capsid formation causes cGAS sensing of viral DNA. *EMBO J* 39: e103958-
771 e103958
772 Sumner RP, Thorne LG, Fink DL, Khan H, Milne RS, Towers GJ (2017) Are Evolution and the
773 Intracellular Innate Immune System Key Determinants in HIV Transmission? *Frontiers in*
774 *immunology* 8: 1246-1246
775 Szabo PA, Dogra P, Gray JI, Wells SB, Connors TJ, Weisberg SP, Krupska I, Matsumoto R, Poon
776 MML, Idzikowski E *et al* (2020) Analysis of respiratory and systemic immune responses in
777 COVID-19 reveals mechanisms of disease pathogenesis. *medRxiv : the preprint server for health*
778 *sciences*
779 Totura AL, Baric RS (2012) SARS coronavirus pathogenesis: host innate immune responses and
780 viral antagonism of interferon. *Current opinion in virology* 2: 264-275
781 Treibel TA, Manisty C, Burton M, McKnight Á, Lambourne J, Augusto JB, Couto-Parada X, Cutino-
782 Moguel T, Noursadeghi M, Moon JC (2020) COVID-19: PCR screening of asymptomatic health-
783 care workers at London hospital. *Lancet (London, England)* 395: 1608-1610
784 Wang LF, Eaton BT (2007) Bats, civets and the emergence of SARS. *Current topics in*
785 *microbiology and immunology* 315: 325-344
786 Williamson EJ, Walker AJ, Bhaskaran K, Bacon S, Bates C, Morton CE, Curtis HJ, Mehrkar A,
787 Evans D, Inglesby P *et al* (2020) Factors associated with COVID-19-related death using
788 OpenSAFELY. *Nature* 584: 430-436
789 Wolff D, Nee S, Hickey NS, Marschollek M (2020) Risk factors for Covid-19 severity and fatality:
790 a structured literature review. *Infection*
791 Wu B, Peisley A, Richards C, Yao H, Zeng X, Lin C, Chu F, Walz T, Hur S (2013) Structural basis for
792 dsRNA recognition, filament formation, and antiviral signal activation by MDA5. *Cell* 152: 276-
793 289
794 Xia H, Cao Z, Xie X, Zhang X, Chen JY, Wang H, Menachery VD, Rajsbaum R, Shi PY (2020)
795 Evasion of Type I Interferon by SARS-CoV-2. *Cell reports* 33: 108234

Yin X, Riva L, Pu Y, Martin-Sancho L, Kanamune J, Yamamoto Y, Sakai K, Gotoh S, Miorin L, De Jesus PD *et al* (2021) MDA5 Governs the Innate Immune Response to SARS-CoV-2 in Lung Epithelial Cells. *Cell reports* 34: 108628

Yuen CK, Lam JY, Wong WM, Mak LF, Wang X, Chu H, Cai JP, Jin DY, To KK, Chan JF *et al* (2020) SARS-CoV-2 nsp13, nsp14, nsp15 and orf6 function as potent interferon antagonists. *Emerging microbes & infections* 9: 1418-1428

Zang R, Gomez Castro MF, McCune BT, Zeng Q, Rothlauf PW, Sonnek NM, Liu Z, Brulois KF, Wang X, Greenberg HB *et al* (2020) TMPRSS2 and TMPRSS4 promote SARS-CoV-2 infection of human small intestinal enterocytes. *Science immunology* 5

Zhang Q, Bastard P, Liu Z, Le Pen J, Moncada-Velez M, Chen J, Ogishi M, Sabli IKD, Hodeib S, Korol C *et al* (2020) Inborn errors of type I IFN immunity in patients with life-threatening COVID-19. *Science (New York, NY)* 370

Zheng J, Wang Y, Li K, Meyerholz DK, Allamargot C, Perlman S (2021) Severe Acute Respiratory Syndrome Coronavirus 2-Induced Immune Activation and Death of Monocyte-Derived Human Macrophages and Dendritic Cells. *The Journal of infectious diseases* 223: 785-795

Zhou F, Yu T, Du R, Fan G, Liu Y, Liu Z, Xiang J, Wang Y, Song B, Gu X *et al* (2020) Clinical course and risk factors for mortality of adult inpatients with COVID-19 in Wuhan, China: a retrospective cohort study. *Lancet (London, England)* 395: 1054-1062

Figure Legends

Figure 1.SARS-CoV-2 activates delayed innate immune responses in lung epithelial cells (A-H) Measurements of replication and innate immune induction in Calu-3 lung epithelial cells infected with SARS-CoV-2 at MOIs 0.08, 0.4 and 2 $TCID50_{VERO}$/cell. (A) Replication of SARS-CoV-2 genomic and subgenomic E RNAs (qRT-PCR). (B) Quantification of N staining from cells in (A) by flow cytometry. Mean percentage of N-positive of all live-gated cells is shown +/- SEM, n=2. (C) Representative example of immunofluorescence staining of N protein (green) after SARS-CoV-2 infection of Calu-3 at MOI 0.4 $TCID50_{VERO}$/cell, at time points shown. Nuclei (DAPI, blue), cell mask (red). Scale bar represents 50µM. (D) Quantification of N staining in cells in (C) by immunofluorescence . (E) Infectious virus released from cells in (A) determined by TCID50 on Vero.E6 cells. (F-H) Fold induction of (F) interferons (IFNβ, IFNλ1 and IFNλ3) (G) IFN stimulated

832 genes (CXCL10 and IFIT2) or (H) pro-inflammatory mediators (IL-6 and CCL5) each overlaid with
833 SARS-CoV-2 E (qRT-PCR). All data from cells in (A) at MOI 0.4 $TCID50_{VERO}$/cell. (A –H) Means from
834 replicate wells shown +/- SEM n=2, full growth curve is representative of three independent
835 experiments. (I-K) SARS-CoV-2 infection (MOIs 0.04 (closed symbols) and 0.0004 (open symbols)
836 $TCID50_{VERO}$/cell) in Calu-3 cells with addition of 10ng/ml IFNβ before or after infection at time
837 points shown, measured by (I) E RNA copies (J) N positive cells, (K) released virus ($TCID50_{VERO}$/cell)
838 all measured at 24 hpi. Dotted line indicates untreated. Mean +/- SEM, n=3, One-way ANOVA
839 Light and dark blue * indicates significance for high and low MOIs respectively.
840
841 **Figure 2. Peak SARS-CoV-2 replication precedes innate immune activation. (A-I)** (**A,C**)
842 Representative images of NF-κB p65 (**A**) (red) and IRF3 (**C**) (red) nuclear localisation in mock or
843 SARS-CoV-2 infected (MOI 0.4 $TCID50_{VERO}$/cell) Calu-3 cells at 24 hpi. SARS-CoV-2 N protein
844 (green. (**E and G**) Representative images of IL-6 mRNA (E) detected by FISH (red) and N protein
845 (green) , or IFIT1 mRNA **(G)** (green) with N protein (red), both with nuclei (DAPI, blue) in mock or
846 SARS-CoV-2 infected (MOI 0.4 $TCID50_{VERO}$/cell) Calu-3 cells at 24 hpi. **(B, D, F, H, I**) Single cell
847 analysis time course quantifying the Integrated Nuclear Intensity of NF-κB p65 **(B),** IRF3 (**D**) , or
848 overall integrated intensity for IL-6 **(F)** or IFIT1 **(H)** mRNA over time in N protein positive cells and
849 N protein negative cells (I). n=2. Kruskal-Wallis test with Dunn's multiple comparison. * ($p<0.05$),
850 **** ($p<0.0001$). Scale bar represents 50µM. (**J,K**) Secretion of CXCL10 (**J**) and IL-6 (**K**) by infected
851 Calu-3 cells (MOIs 0.08, 0.4 and 2 $TCID50_{VERO}$/cell), (ELISA). (**L**) Lactate dehydrogenase (LDH)
852 release into culture supernatants by mock and SARS-CoV-2 infected Calu-3 cells (MOIs 0.08, 0.4
853 and 2 $TCID_{VERO}50$/cell) quantified absorbance (492nm). **(M**) Quantification of live/dead staining
854 of non-adherent cells recovered from supernatants of mock or SARS-CoV-2 infected Calu-3
855 cultures at 48 and 72hpi. Data information: (J-M) Means from replicate wells shown +/- SEM,
856 n=2, representative of three independent experiments.
857
858 **Figure 3. SARS-CoV-2 is sensed by MDA5 and RIG-I. (A-D)** Measurement of (**A**) viral genomic and
859 subgenomic E RNA at 24 hpi, (**B**) fold induction of CXCL10 from (A), (**C**) IFIT2 and (**D**) IL-6 mRNA
860 (qRT-PCR) from (A) after Remdesivir treatment (0.125-5 µM) of SARS-CoV-2 infected Calu-3 cells

861 (MOI 0.04 TCID50/cell) with Remdesivir added 2h prior to infection. Mean +/- SEM, n=3. (**E-H**)
862 Measurement of (**E**) viral genomic and subgenomic E RNA (**F**) fold induction of CXCL10, **(G)** IFIT2
863 and (**H**) and IL-6 at 24 hpi, of Calu-3 cells with SARS-CoV-2 (MOI 0.04 $TCID50_{VERO}$/cell) with
864 Remdesivir treatment (5µM) prior to, at the time of, or 8 h post-infection. Mean +/- SEM, n=3,
865 One way ANOVA with Dunnett's multiple comparisons test to compare to untreated infected
866 condition ('mock'), ** (p<0.01), *** (p<0.001), **** (p<0.0001). (**I**) Representative example of
867 immunofluorescence staining of dsRNA (red) and N protein (green) after SARS-CoV-2 infection of
868 Calu-3 at MOI 0.4 $TCID50_{VERO}$/cell, at time points shown. Nuclei (DAPI, blue). Scale bar represents
869 50µM. **(J)** RNAi mediated depletion of MAVS, RIG-I or MDA-5, reduced their expression levels as
870 compared to siControl (siCtrl) Mean +/- SEM, n=3. Two-Way ANOVA with Sidak's multiple
871 comparisons test, **** (p<0.0001). (**K-O**) Fold induction of (**K**) IFNβ, (**L**) CXCL10, (**M**) IFIT2 (**N**) TNF
872 and **(O)** IL-6 or in SARS-CoV-2 infected Calu-3 cells (MOI 0.04 TCID50/cell) 24 hpi. Mean +/- SEM,
873 n=3, and compared to siCtrl for each gene by One Way ANOVA with Dunnett's multiple
874 comparisons test, ** (p<0.01), *** (p<0.001), **** (p<0.0001), n.s. : non significant. (**P**) Live/dead
875 stain counts for non-adherent cells, recovered at 48 hpi from supernatants of SARS-CoV-2
876 infected Calu-3 cells, depleted for MAVS or RNA sensors, compared to siCtrl. Non-adherent cell
877 counts were determined by acquisition by flowcytometry for a defined period of time. Mean +/-
878 SEM, n=3. Total numbers are compared to siCtrl by unpaired t-test, *** (p<0.001). (**Q-R**) (**Q**) Viral
879 E RNA and (**R**) released infectious virus ($TCID50_{VERO}$/cell) at 24 hpi of infected Calu-3 cells depleted
880 for MAVs, RIG-I or MDA5. Mean +/- SEM, n=3. Each group compared to siCtrl by One Way ANOVA
881 with Dunnett's multiple comparisons test, *, p>0.05, ** (p<0.01), n.s : non significant.
882
883 **Figure 4. NF-κB and JAK/STAT signalling drive innate immune responses.** (**A-C**) Fold induction
884 at 24 hpi of (**A**) CXCL10, **(B)** IFIT1 or (**C**) IL-6 mRNA (qRT-PCR) after Calu-3 infection with SARS-
885 CoV-2 over a range of MOIs (0.004, 0.04, 0.4 $TCID50_{VERO}$/cell) in the presence of 10 µM TPCA-1 or
886 DMSO as shown. (**D-F**) Fold induction at 24 hpi of (**D**) CXCL10, **(E)** IFIT2 or (**F**) IL-6 mRNA (RT-qPCR)
887 after Calu-3 infection with SARS-CoV-2 over a range of MOIs (0.0004, 0.004, 0.04, 0.4
888 $TCID50_{VERO}$/cell) in the presence of 2 µM Ruxolitinib (Rux) or DMSO as shown. (**G-H**) Viral genomic
889 and subgenomic E RNA at 24 hpi (RT-qPCR) with DMSO or TPCA (G) or Rux (H) treatment. Data

890 information: (A-H) Mean +/- SEM, n=3, statistical comparisons are made by unpaired t test
891 comparing inhibitor-treated to mock-treated SARS-CoV-2 infected conditions at each MOI and
892 each timepoint. * ($p<0.05$), ** ($p<0.01$), *** ($p<0.001$), **** ($p<0.0001$). (**I**) Live/dead stain count
893 from non-adherent cells recovered from supernatants of SARS-CoV-2 infected Calu-3 cultures
894 (MOI 0.04 $TCID50_{VERO}$/cell) 48hpi (flow cytometry). Mean +/- SEM, (n=3). One Way ANOVA
895 comparison of inhibitor-treated infected cells to mock-treated infected cells. *** ($p<0.001$).
896
897 **Figure 5. Epithelial responses to SARS-CoV-2 drive macrophage activation** (**A**) Schematic of
898 experimental design. (**B-J**) Calu-3 cells were transfected with siRNA targeting MAVS or non-
899 targeting control (siCtrl) (B-D) or treated with DMSO vehicle or inhibitors 10 µM TPCA-1 (E-G) or
900 2 µM Ruxolitinib (Rux) (H-J) as shown, and were mock-infected or infected with SARS-CoV-2 at
901 MOI 0.04 $TCID50_{VERO}$/cell. Virus containing conditioned media (CoM) was harvested at 48 hpi.
902 MDM were treated with Calu-3 virus containing CoM for 6 hpi, before washing and measuring
903 MDM gene expression (B, E, H), and MDM activation markers by flowcytometry 48 h later
904 (C,D,F,G,I,J) , plotting relative median fluorescent intensity (MFI) compared to mock-infected
905 siCtrl (C, D) or mock-infected DMSO control (F, G, I, J). Legends in (B), (E) and (H) apply to (C,D),
906 (F,G) and (I,J) respectively. The inhibitors in (E) and (H) were tested side-by-side with the same
907 mock condition. Mean +/- SEM shown, data from 4-6 independent MDM donors is shown.
908 Statistical comparison by two-tailed paired t-test comparing MDM exposed to control infected
909 CoM to siMAVS/inhibitor treated infected CoM. * ($p<0.05$), ** ($p<0.01$), *** ($p<0.001$). **(K-O)**
910 MDM were treated with either anti-IFNAR antibody (2.5ug/ml), an isotype control IgG antibody
911 (IgG, 2.5ug/ml), Rux (2 µM), or mock treated during 6 h of exposure to CoM from infected,
912 unmodified Calu-3 cells, before washing and measuring MDM gene expression (K, L, M), and
913 MDM activation markers (N, O) by flowcytometry 48 h later. Both gene expression and relative
914 MFI are compared to mock-treated MDM exposed to CoM from uninfected Calu-3s cells. Mean
915 +/- SEM shown, data from 7-8 independent MDM donors is shown. Statistical testing by one-way
916 paired ANOVA, comparing treated MDMs to untreated control by Dunnett's multiple comparison
917 test, * ($p<0.05$), ** ($p<0.01$), *** ($p<0.001$).
918

919 **Figure 6. Pre-existing immune activation exacerbates SARS-CoV-2-dependent inflammation.**
920 (**A**) Schematic of experimental design. (**B-H**) MDM were primed with 100ng/ml LPS for 2h before
921 exposure to SARS-CoV-2 (MOI 0.02 $TCID50_{VERO}$/cell). (**B**) Expression of genomic and subgenomic
922 viral E RNA at 48 h post exposure in indicated conditions. (**C-G**) Host gene expression of (**C**) CCL5,
923 (**D**) ISG56, (**E**) IFIT2, (**F**) IL-6 or (**G**) IL-1b was measured 48hpi. (**H**) IL-1b secretion was detected in
924 culture supernatants at 48 hpi by ELISA. (**I**) Schematic of experimental design. MDM were
925 exposed to SARS-CoV-2 (MOI 0.02 $TCID50_{VERO}$/cell) for 48 h and subsequently stimulated with
926 100ng/ml LPS for 24 h. **(J-P)** (**J**) Expression of genomic and subgenomic viral E RNA 72 h post-
927 exposure in indicated conditions. (**K-O**) Host gene expression of (**K**) CCL5, (**L**) ISG56, (**M**) IFIT2, (**N**)
928 IL-6 and (**O**) IL-1b. (**P**) IL-1b secretion was detected in culture supernatants at 48 hpi by ELISA.
929 Data Information: (A-P) Gene expression is shown as fold induction over untreated controls. Data
930 from 8-13 independent donors is shown. Groups were compared as indicated by Wilcoxon
931 matched-pairs signed rank test, *, $p<0.05$, ** ($p<0.01$), *** ($p<0.001$). (**Q-V**) Calu-3 cells were
932 infected with SARS-CoV-2 (MOI 0.04 $TCID50_{VERO}$/cell) in the presence or absence of 10ng/ml IL-
933 1b. (**Q-T**) Gene expression of (**Q**) IFNβ (**R**), CXCL10, (**S**) IL-6 and (**T**) IFIT1 was measured after 24h.
934 Fold induction over untreated mock infection is shown, n=3. (**U**) Non-adherent cells were
935 collected at 48h post infection and live/dead stained. Cells were acquired by flowcytometry and
936 cell counts determined by time-gating. For statistical comparison, total cell numbers were
937 compared. (**V**) Viral release into culture supernatants at 24 h was measured by TCID50 on VeroE6
938 cells. (**Q-V**) Mock and SARS-CoV-2 infected conditions were compared with or without IL1b-
939 treatment, respectively, by unpaired T test (n=3). *, $p<0.05$; n.s., non-significant. Mean +/- SEM
940 shown.
941
942 **Figure 7. SARS-CoV-2 induces a delayed inflammatory response that can be modified by specific**
943 **pathway inhibitors.** (Left) Infected lung epithelial cells sense SARS-CoV-2 RNA via cytoplasmic
944 RNA sensors RIG-I and MDA5 to activate secretion of inflammatory mediators. Manipulation of
945 RNA sensing early in infection by viral innate immune antagonists leads to a delayed and
946 particularly inflammatory response. The infected cell secretome activates macrophages to
947 potentiate an pro-inflammatory state at the site of infection. (Right) Inhibition of RNA sensing or

948 downstream signalling pathways, for example with NF-κB inhibitors, reduces inflammation in
949 infected cells and consequent activation of pro-inflammatory macrophages.
950
951 **Expanded view Figure Legends**
952
953 **Figure EV1. SARS-CoV-2 replication in Caco-2 cells does not induce an innate response.** (**A**)
954 Immunoblot detecting ACE2 expression in epithelial (Detroit 562, Beas2B, Calu-3, Caco-2),
955 endothelial (HULEC5a) and PMA-differentiated THP-1 cells. b-Actin is detected as loading control.
956 (**B**) *ACE2*, *TMPRSS2* and *TMPRSS4* gene expression in cell lines and primary monocyte-derived
957 macrophages (MDM). Relative expression normalised to *GAPDH* Mean +/- SEM n=2. (**C-G**)
958 Measurements of replication and innate immune induction in Caco-2 intestinal epithelial cells
959 infected with SARS-CoV-2 at MOI 0.08, 0.4 or 2 $TCID50_{VERO}$/cell. Mean +/- SEM, n=2. (**C**) SARS-
960 CoV-2 genomic and subgenomic E RNAs (qRT-PCR). (**D**) Infectious virus released from cells in (C)
961 determined by TCID50 on Vero.E6 cells, Mean +/-SEM n=2. (**E**) Quantification of N staining from
962 cells in (C) by flow cytometry. Mean percentage of N-positive of all live-gated cells +/- SEM, n=2.
963 (**F**) Representative example of immunofluorescence staining of N protein (green) after SARS-CoV-
964 2 infection of Caco-2 at MOI 0.4 $TCID50_{VERO}$/cell, at time points shown. Nuclei (DAPI, blue), cell
965 mask (red). (**G**) Fold induction of interferon and interferon stimulated genes (ISG) of infections in
966 (C) at 24h and 72 hpi at MOIs $TCID50_{VERO}$/cell 0.08, 0.4 or 2, n=2. (**H**) Fold induction of ISG and
967 cytokine gene expression in Caco-2 cells in response to innate immune activation with polyI:C,
968 R837 and LPS for 24 h, n=2. (**I**) Fold induction of ISG and cytokine gene expression in Calu-3 cells
969 in response to innate immune activation with polyI:C (+/- transfection, TF), R837 and LPS for 24
970 h, n=2. Mean +/- SEM.
971
972 **Figure EV2. SARS-CoV-2 replicates rapidly in Calu-3 cells and induces a delayed innate response.**
973 (**A-C**) Measurements of viral replication in Calu-3 lung epithelial cells infected with SARS-CoV-2
974 at MOIs 0.0004, 0.004, 0.04 or 0.4 $TCID50_{VERO}$/cell, n=3. (**A**) Replication of SARS-CoV-2 genomic
975 and subgenomic E RNAs (qRT-PCR). (**B**) Quantification of N protein-positive cells from (A) by flow
976 cytometry. Mean percentage of N +ve of all live-gated cells. (**C**) Infectious virus released from

977 cells in (A) determined by TCID50 on Vero.E6 cells. (**D**) Fold induction of Chemokines from
978 infections in (Figure 1) (*CCL5*, *CXCL10*, *CCL2*, *CCL3*), Cytokines (*IL-8*, *IL-6*, *IL-1*β, *IL1*α, *TNF*),
979 Interferons (*IFN*β, *IFNλ1*, *IFNλ3*) and ISGs (*IFIT2*, *MX1*, *IFIT1*) at 24 hpi in Calu-3 cells infected at
980 MOIs 0.08, 0.4 or 2 $TCID50_{VERO}$/cell, n=2. (**E**) Fold induction of *IFIT2*, *CCL5*, *CXCL10*, *IL6*, *IFN*β,
981 *IFNλ1*, *IFNλ3* in Calu-3 cells at MOI 0.08 or 2 $TCID50_{VERO}$/cell each overlaid with SARS-CoV-2 E
982 (qRT-PCR), n=2. (**F**) Fold induction of *CXCL10*, *IL-6* and *IFIT1* in SARS-CoV-2 infected Calu-3 cells
983 from (A) at MOIs 0.0004, 0.004, 0.04 or 0.4 $TCID50_{VERO}$/cell, n=3. (**G**) SARS-CoV-2 infection (MOIs
984 0.04 $TCID50_{VERO}$/cell) in Calu-3 cells after addition of 10 ng/ml IFNβ, IFNλ1, IFNλ2 or IFNγ before
985 or after infection at time points shown, measured by E RNA copies, N-positive cells (relative to
986 untreated infection) and released virus as $TCID50_{VERO}$/ml, all measured at 24 hpi. Treatments
987 were compared to untreated SARS-CoV-2 infected Calu-3 cells by T test. *, $p<0.05$; **, $p<0.01$;
988 ***, $p<0.001$ or exact p-value are shown. Mean +/- SEM shown, n=3. (**H**) Fold induction of *CXCL10*
989 and *IFIT1* in interferon-treated Calu-3 cells at 24h. Means +/- SEM, n=3.
990
991 **Figure EV3. NF-κB and IRF3 translocation in SARS-CoV-2 infected cells. (A)** Single cell analysis
992 time course quantifying the Integrated Nuclear Intensity of NF-κB p65 or IRF3 in SARS-CoV-2
993 infected Calu-3 cells at MOI 2, 0.4 or 0.04 $TCID50_{VERO}$/cell or mock infected as labelled. At all
994 timepoints, nuclear intensities of NF-κB or IRF3 in nucleocapsid protein-positive infected cells
995 (blue) and N-ve cells (grey) are shown. Nuclear Intensities of uninfected cells (Mock) at 24 h are
996 shown as comparator. All MOIs and mocks were performed side-by-side and the mock is the
997 same within panels for N NF-κB and within the IRF3 panels. Horizontal lines indicate the mean.
998 Kruskal-Wallis test with Dunn's multiple comparison, *, $p<0.05$; **, $p<0.01$; ***, $p<0.001$.
999
1000 **Figure EV4. SARS-CoV-2 activation of the innate response in Calu-3 cells coincides with**
1001 **inflammatory cell death.** (**A**) Representative single cell RNA FISH analysis time course quantifying
1002 the Integrated Intensity of *IL-6* in uninfected (Mock) or uninfected bystander cells (uninfected
1003 cells, grey) of Calu-3 cells infected at MOI 0.4 TCID50/cell. (**B**) Representative single cell RNA FISH
1004 analysis time course quantifying the Integrated Intensity of *GAPDH* in uninfected (Mock),
1005 nucleocapsid protein-positive infected (blue) and uninfected bystander (grey) Calu-3 cells at MOI

1006 0.4 TCID50/cell. (**A,B**) Horizontal lines indicate the median with Kruskal-Wallis test with Dunn's
1007 multiple comparison, *, p<0.05; **, p<0.01; ***, p<0.001. (**C**) Secretion of IL-6 and CXCL10 (ELISA)
1008 by infected Calu-3 cells (MOIs 0.0004, 0.004, 0.04 and 0.4 $TCID50_{VERO}$/cell), matching infections
1009 in Figure EV2A-C and F. Mean +/- SEM, n=3. (**D**) Lactate dehydrogenase (LDH) release into culture
1010 supernatants by mock and SARS-CoV-2 infected Calu-3 cells (MOIs 0.0004, 0.004, 0.04 and 0.4
1011 $TCID50_{VERO}$/cell, matching infections in Figure 2A-C and F) quantified by absorbance (492nm),
1012 means +/- SEM, n=3, (**E**) Representative flowcytometry contour plots depicting intracellular
1013 nucleocapsid protein detection (Cr3009-AlexaFluor488) and Live/Dead (Live/Dead-UV) staining.
1014 Shown are infected (MOI 0.04 $TCID50_{VERO}$ /cell) and uninfected (Mock) Calu-3 cells at 48h post
1015 infection. Adherent and non-adherent cells were collected and acquired. (**F**) Quantification of
1016 Live/Dead staining of non-adherent cells recovered from supernatants of Mock or SARS-CoV-2
1017 infected Calu-3 cultures (MOIs 0.0004, 0.004, 0.04 and 0.4 $TCID50_{VERO}$/cell) at 24, 48 or 72 hpi.
1018 Mean +/- SEM, n=3.
1019
1020 **Figure EV 5. Inhibition of IFN and NF-κB signalling reduces the inflammatory response during**
1021 **SARS-CoV-2 infection**. **(A-C)** Fold gene induction of *IL-6, CXCL10* and *IFIT1* 24hpi of Calu-3 with
1022 SARS-CoV-2 (MOI 0.04 $TCID50_{VERO}$/celll) infected in the presence of: **(A)** 10 µM TPCA-1 (**B**) 10 µM
1023 PS1145 or (**C**) 10 µM Ruxolitinib (Rux) with DMSO as control in each case. (**D-F**) Measurement of
1024 SARS-CoV-2 (MOI 0.04 $TCID50_{VERO}$/cell) replication in Calu-3 in the presence or absence of 10 µM
1025 TPCA-1, 10 µM Ruxolitinib (Rux) or DMSO vehicle as shown measuring (**D**) genomic and
1026 subgenomic E RNA, (**E**) N +ve cells by flow cytometry, (**F**) released virus in supernatant
1027 ($TCID50_{VERO}$/cell) at 24 hpi. Mock and SARS-CoV-2 infected/treated conditions were compared by
1028 two tailed t test. *, p<0.05; **, p<0.01; n.s., non-significant. Mean +/- SEM, n=3.

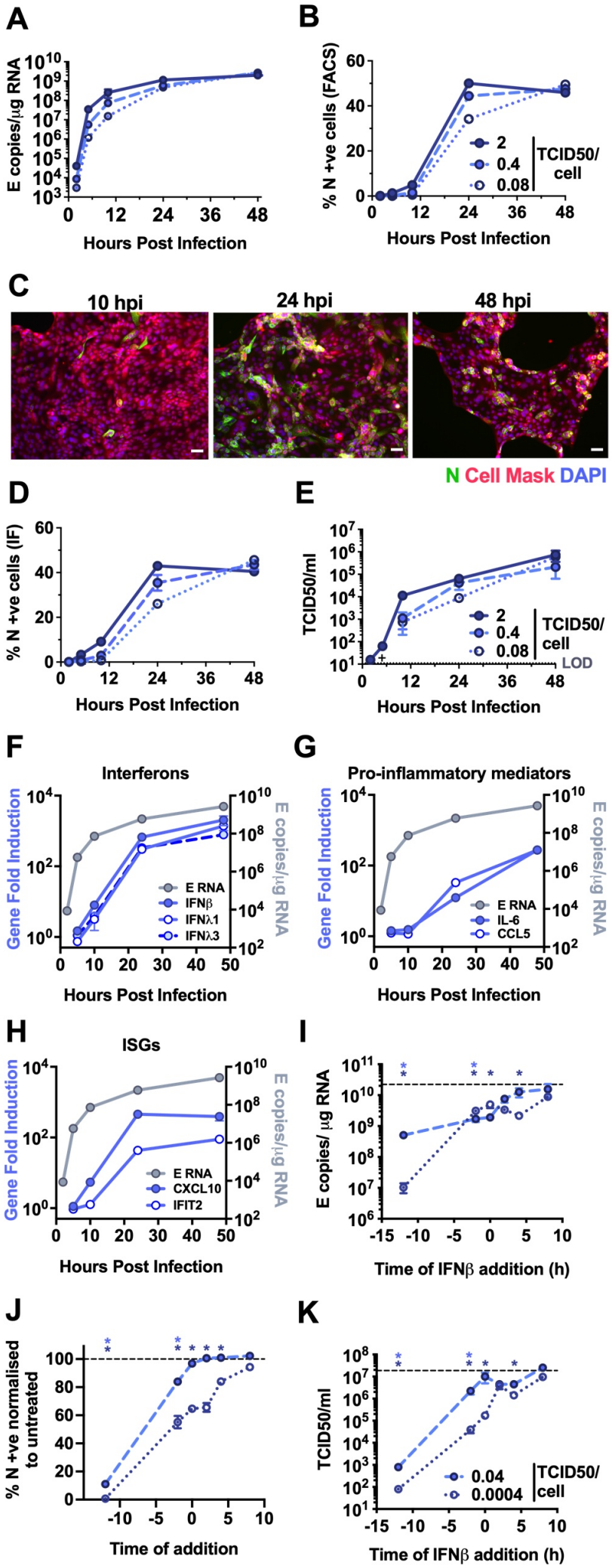
A
E copies/µg RNA
Hours Post Infection
B
% N +ve cells (FACS)
2
0.4
0.08
TCID50/ cell
Hours Post Infection
C
10 hpi
24 hpi
48 hpi
N Cell Mask DAPI
D
% N +ve cells (IF)
Hours Post Infection
E
TCID50/ml
2
0.4
0.08
TCID50/ cell
LOD
Hours Post Infection
F
Interferons
Gene Fold Induction
E copies/µg RNA
E RNA
IFNβ
IFNλ1
IFNλ3
Hours Post Infection
G
Pro-inflammatory mediators
Gene Fold Induction
E copies/µg RNA
E RNA
IL-6
CCL5
Hours Post Infection
H
ISGs
Gene Fold Induction
E copies/µg RNA
E RNA
CXCL10
IFIT2
Hours Post Infection
I
E copies/ µg RNA
Time of IFNβ addition (h)
J
% N +ve normalised to untreated
Time of addition
K
TCID50/ml
0.04
0.0004
TCID50/ cell
Time of IFNβ addition (h)

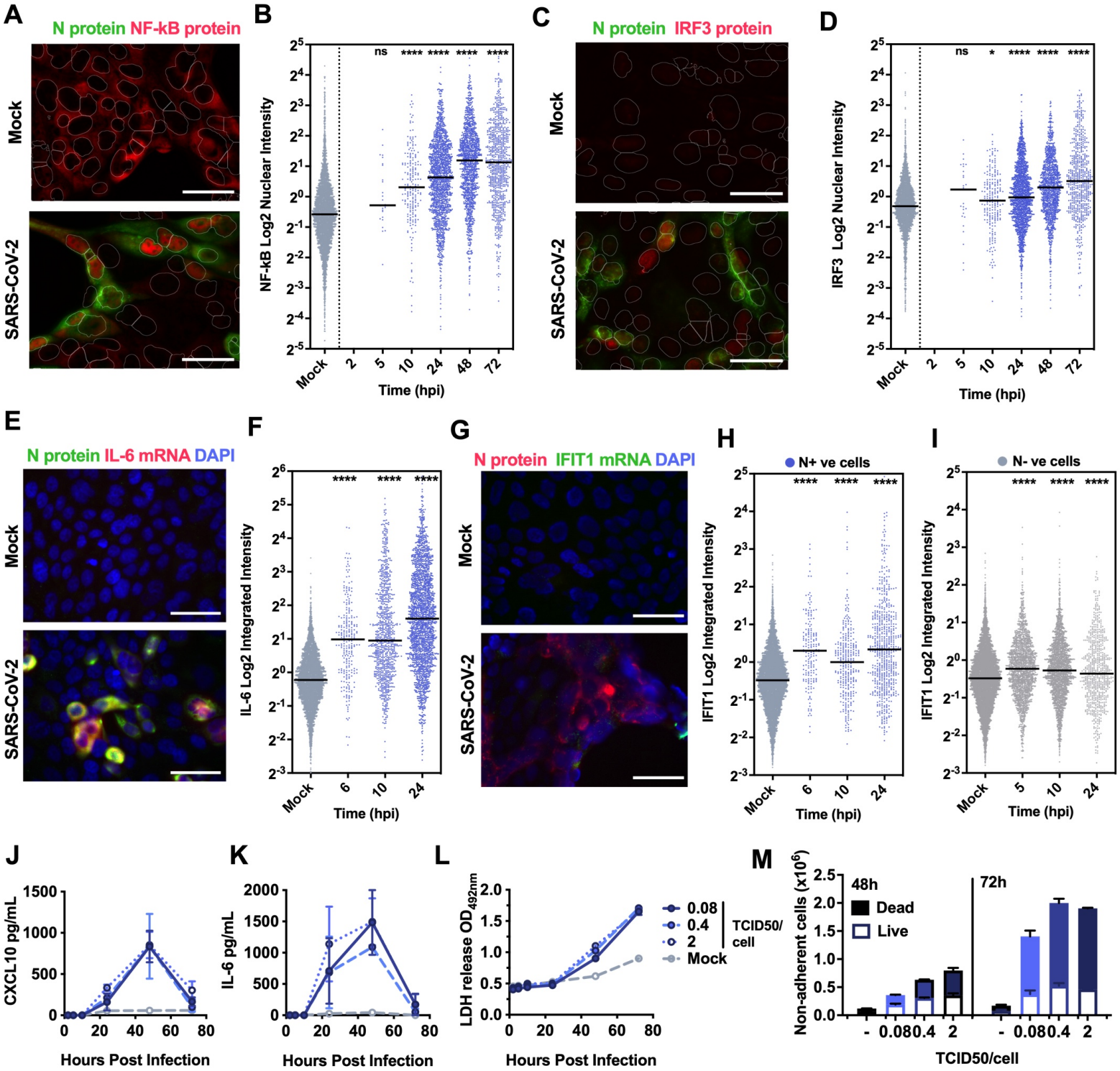
A
N protein NF-kB protein
Mock
SARS-CoV-2
B
NF-kB Log2 Nuclear Intensity
ns
****
Mock
2
5
10
24
48
72
Time (hpi)
C
N protein IRF3 protein
Mock
SARS-CoV-2
D
IRF3 Log2 Nuclear Intensity
ns
*
****
Time (hpi)
E
N protein IL-6 mRNA DAPI
Mock
SARS-CoV-2
F
IL-6 Log2 Integrated Intensity
****
Mock
6
10
24
Time (hpi)
G
N protein IFIT1 mRNA DAPI
Mock
SARS-CoV-2
H
N+ ve cells
IFIT1 Log2 Integrated Intensity
Time (hpi)
I
N- ve cells
IFIT1 Log2 Integrated Intensity
Time (hpi)
J
CXCL10 pg/mL
Hours Post Infection
K
IL-6 pg/mL
Hours Post Infection
L
LDH release OD492nm
0.08
0.4
2
Mock
TCID50/ cell
Hours Post Infection
M
Non-adherent cells (x10^6)
48h
72h
Dead
Live
TCID50/cell

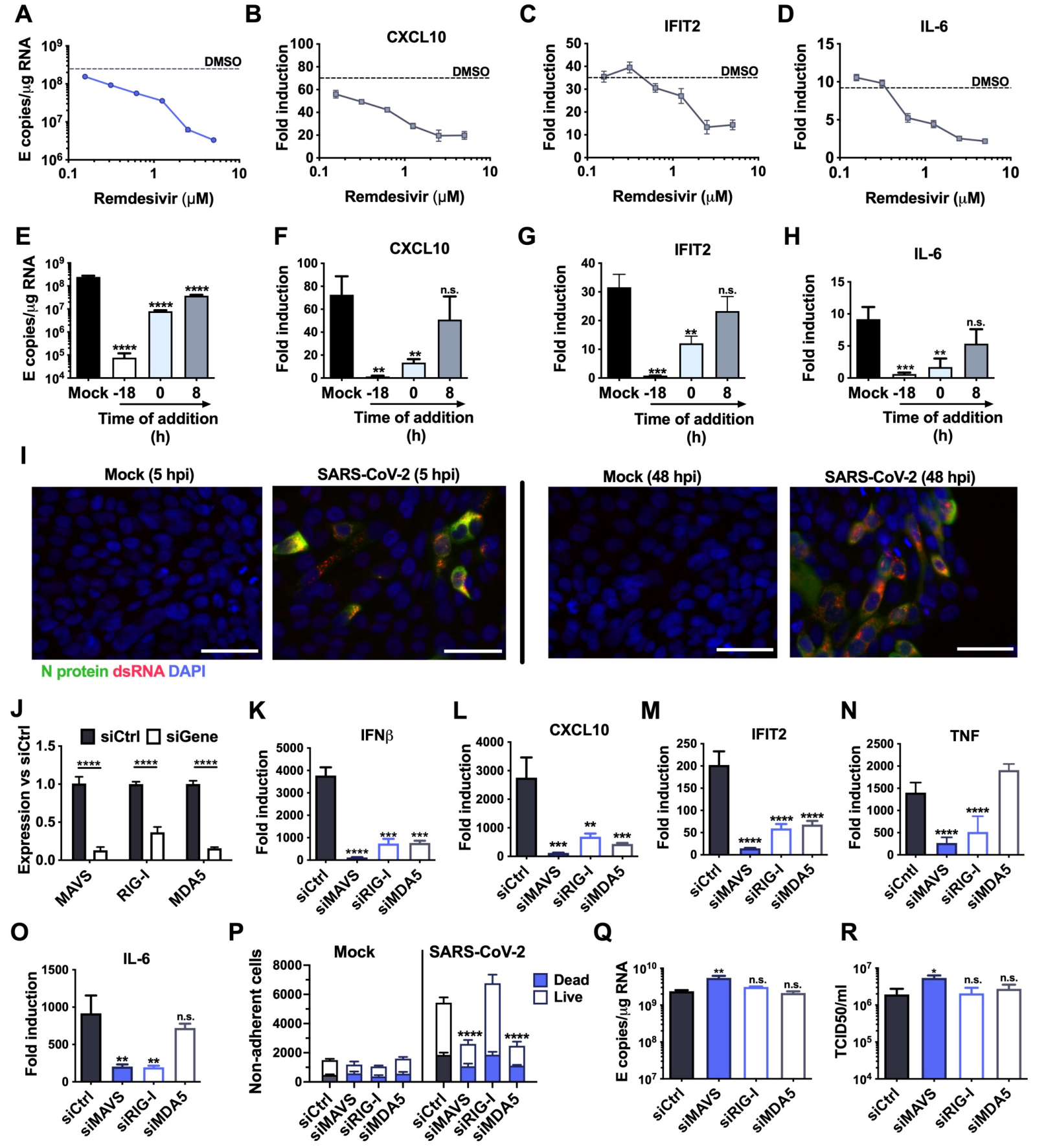
A
E copies/μg RNA
DMSO
Remdesivir (μM)
B
CXCL10
Fold induction
DMSO
Remdesivir (μM)
C
IFIT2
Fold induction
DMSO
Remdesivir (μM)
D
IL-6
Fold induction
DMSO
Remdesivir (μM)
E
E copies/μg RNA
Mock -18 0 8
Time of addition (h)
F
CXCL10
Fold induction
Mock -18 0 8
Time of addition (h)
G
IFIT2
Fold induction
Mock -18 0 8
Time of addition (h)
H
IL-6
Fold induction
Mock -18 0 8
Time of addition (h)
I
Mock (5 hpi)
SARS-CoV-2 (5 hpi)
Mock (48 hpi)
SARS-CoV-2 (48 hpi)
N protein dsRNA DAPI
J
siCtrl siGene
Expression vs siCtrl
MAVS RIG-I MDA5
K
IFNβ
Fold induction
siCtrl siMAVS siRIG-I siMDA5
L
CXCL10
Fold induction
siCtrl siMAVS siRIG-I siMDA5
M
IFIT2
Fold induction
siCtrl siMAVS siRIG-I siMDA5
N
TNF
Fold induction
siCntl siMAVS siRIG-I siMDA5
O
IL-6
Fold induction
siCtrl siMAVS siRIG-I siMDA5
P
Mock
SARS-CoV-2
Dead
Live
Non-adherent cells
siCtrl siMAVS siRIG-I siMDA5
Q
E copies/μg RNA
siCtrl siMAVS siRIG-I siMDA5
R
TCID50/ml
siCtrl siMAVS siRIG-I siMDA5

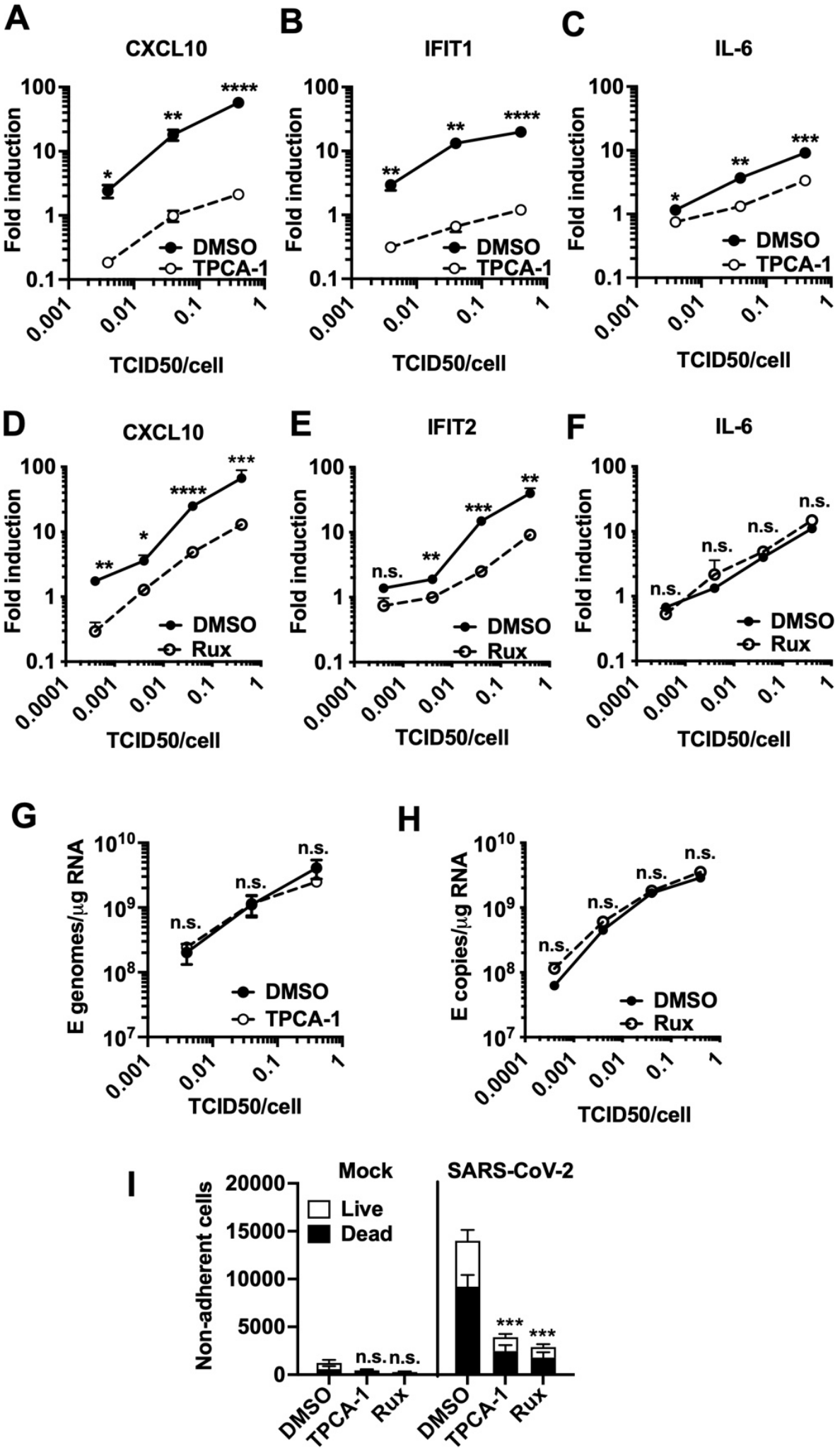
A
CXCL10
Fold induction
TCID50/cell
DMSO
TPCA-1
B
IFIT1
C
IL-6
D
CXCL10
Rux
E
IFIT2
F
IL-6
G
E genomes/μg RNA
H
E copies/μg RNA
I
Mock
SARS-CoV-2
Live
Dead
Non-adherent cells
n.s.

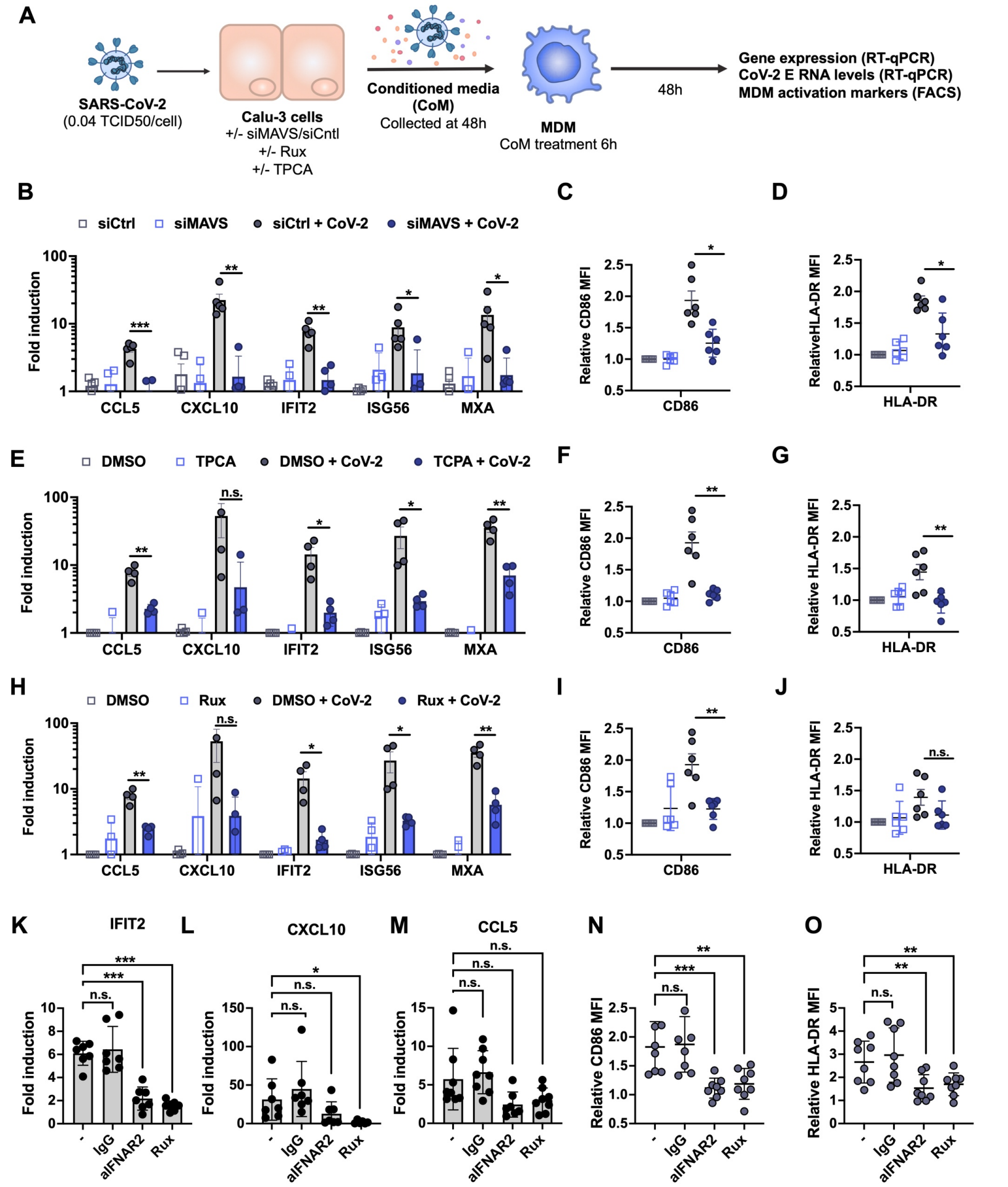
A
SARS-CoV-2
(0.04 TCID50/cell)
Calu-3 cells
+/- siMAVS/siCntl
+/- Rux
+/- TPCA
Conditioned media
(CoM)
Collected at 48h
MDM
CoM treatment 6h
48h
Gene expression (RT-qPCR)
CoV-2 E RNA levels (RT-qPCR)
MDM activation markers (FACS)
B
siCtrl
siMAVS
siCtrl + CoV-2
siMAVS + CoV-2
Fold induction
CCL5
CXCL10
IFIT2
ISG56
MXA
C
Relative CD86 MFI
CD86
D
RelativeHLA-DR MFI
HLA-DR
E
DMSO
TPCA
DMSO + CoV-2
TCPA + CoV-2
F
G
H
DMSO
Rux
DMSO + CoV-2
Rux + CoV-2
I
J
Relative HLA-DR MFI
K
IFIT2
L
CXCL10
M
CCL5
N
O
-
IgG
aIFNAR2
Rux

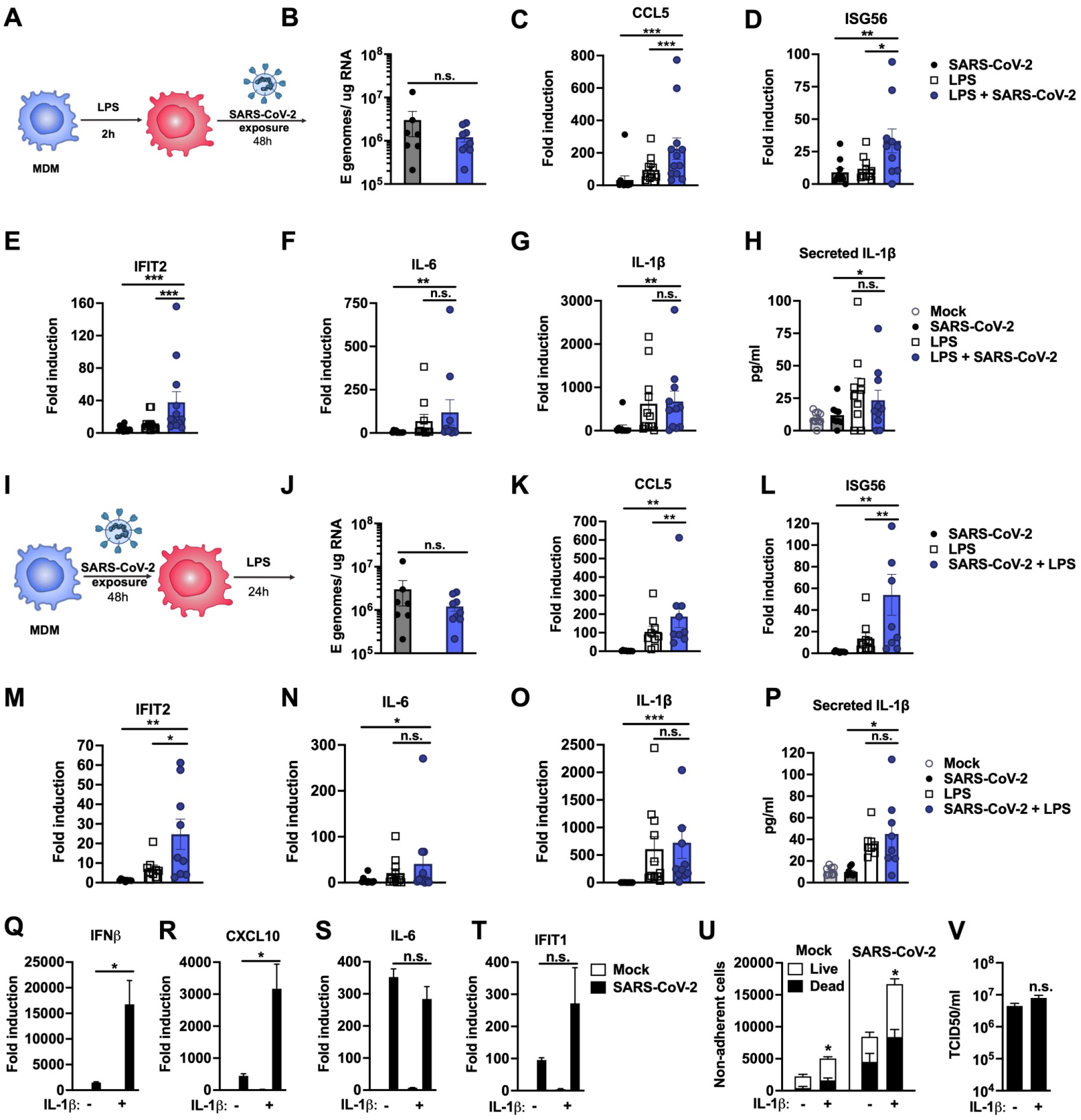
A
MDM
LPS
2h
SARS-CoV-2
exposure
48h
B
E genomes/ ug RNA
n.s.
C
CCL5
Fold induction
D
ISG56
Fold induction
SARS-CoV-2
LPS
LPS + SARS-CoV-2
E
IFIT2
Fold induction
F
IL-6
Fold induction
G
IL-1β
Fold induction
H
Secreted IL-1β
pg/ml
Mock
SARS-CoV-2
LPS
LPS + SARS-CoV-2
I
MDM
SARS-CoV-2
exposure
48h
LPS
24h
J
E genomes/ ug RNA
n.s.
K
CCL5
Fold induction
L
ISG56
Fold induction
SARS-CoV-2
LPS
SARS-CoV-2 + LPS
M
IFIT2
Fold induction
N
IL-6
Fold induction
O
IL-1β
Fold induction
P
Secreted IL-1β
pg/ml
Mock
SARS-CoV-2
LPS
SARS-CoV-2 + LPS
Q
IFNβ
Fold induction
IL-1β: - +
R
CXCL10
Fold induction
IL-1β: - +
S
IL-6
Fold induction
n.s.
IL-1β: - +
T
IFIT1
Fold induction
n.s.
IL-1β: - +
Mock
SARS-CoV-2
U
Mock
SARS-CoV-2
Live
Dead
Non-adherent cells
IL-1β: - + - +
V
TCID50/ml
n.s.
IL-1β: - +

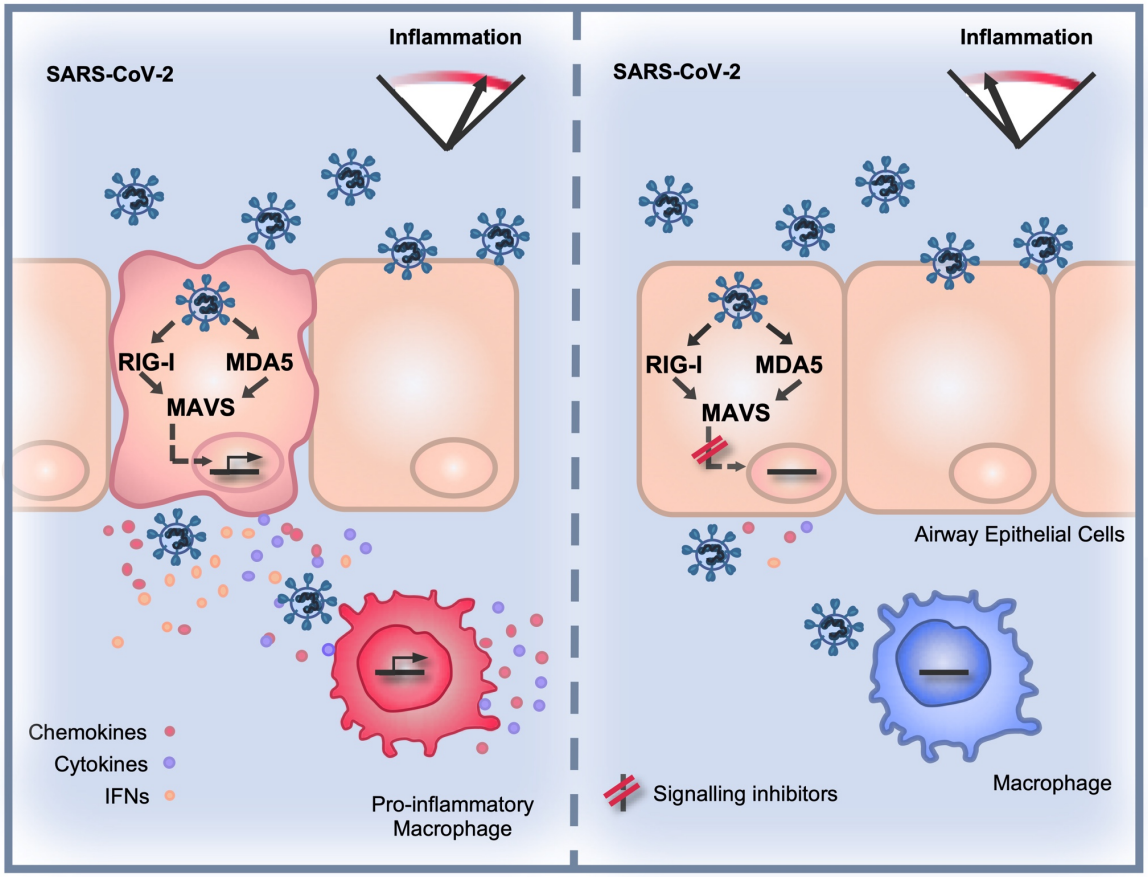
Inflammation
SARS-CoV-2
RIG-I
MDA5
MAVS
Chemokines
Cytokines
IFNs
Pro-inflammatory
Macrophage
Inflammation
SARS-CoV-2
RIG-I
MDA5
MAVS
Airway Epithelial Cells
Signalling inhibitors
Macrophage

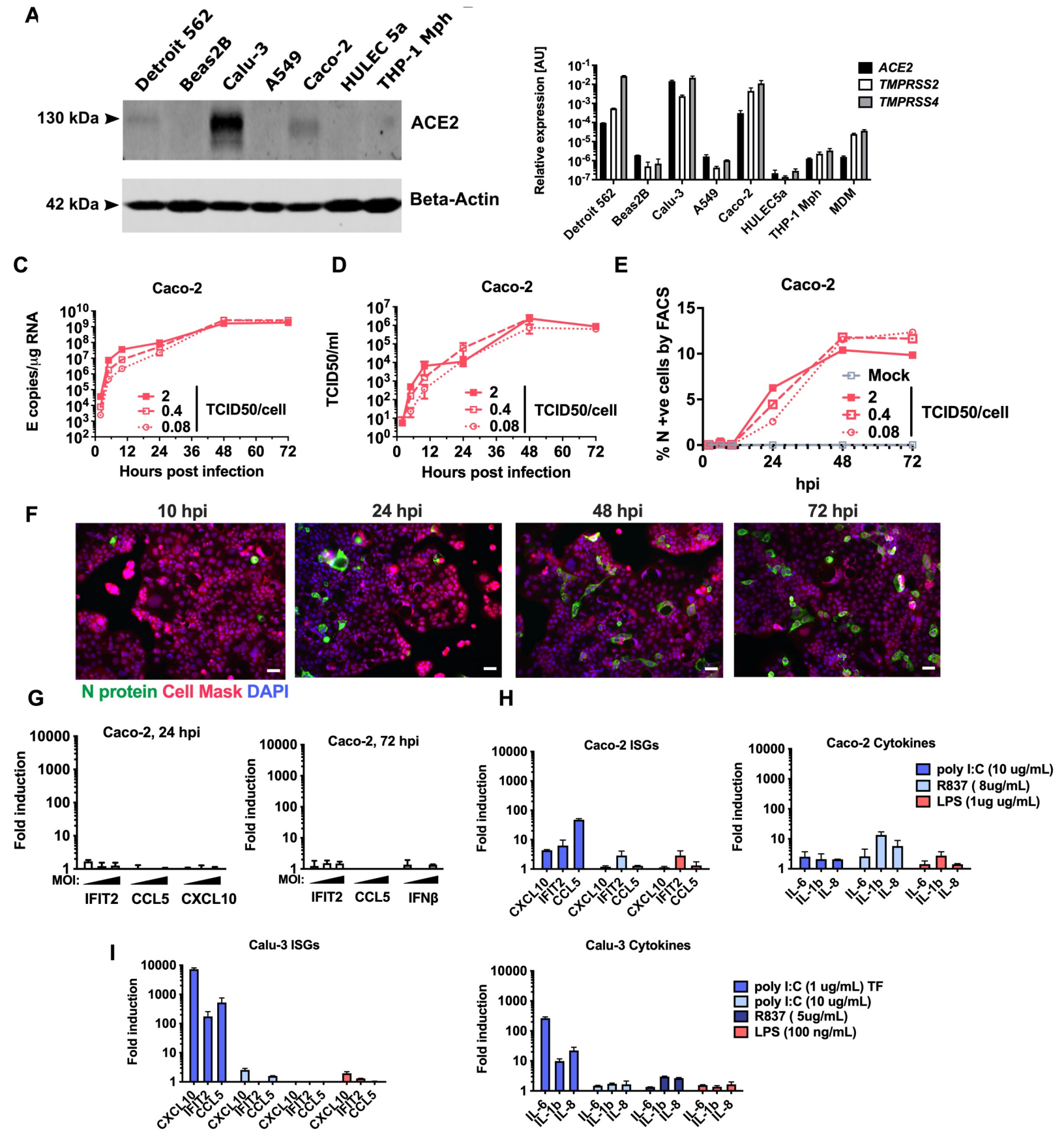
A
Detroit 562
Beas2B
Calu-3
A549
Caco-2
HULEC 5a
THP-1 Mph
130 kDa
ACE2
42 kDa
Beta-Actin
Relative expression [AU]
ACE2
TMPRSS2
TMPRSS4
Detroit 562
Beas2B
Calu-3
A549
Caco-2
HULEC5a
THP-1 Mph
MDM
C
Caco-2
E copies/µg RNA
2
0.4
0.08
TCID50/cell
Hours post infection
D
Caco-2
TCID50/ml
2
0.4
0.08
TCID50/cell
Hours post infection
E
Caco-2
% N +ve cells by FACS
Mock
2
0.4
0.08
TCID50/cell
hpi
F
10 hpi
24 hpi
48 hpi
72 hpi
N protein Cell Mask DAPI
G
Caco-2, 24 hpi
Fold induction
MOI:
IFIT2
CCL5
CXCL10
Caco-2, 72 hpi
Fold induction
MOI:
IFIT2
CCL5
IFNβ
H
Caco-2 ISGs
Fold induction
CXCL10
IFIT2
CCL5
Caco-2 Cytokines
Fold induction
poly I:C (10 ug/mL)
R837 (8ug/mL)
LPS (1ug ug/mL)
IL-6
IL-1b
IL-8
I
Calu-3 ISGs
Fold induction
CXCL10
IFIT2
CCL5
Calu-3 Cytokines
Fold induction
poly I:C (1 ug/mL) TF
poly I:C (10 ug/mL)
R837 (5ug/mL)
LPS (100 ng/mL)
IL-6
IL-1b
IL-8

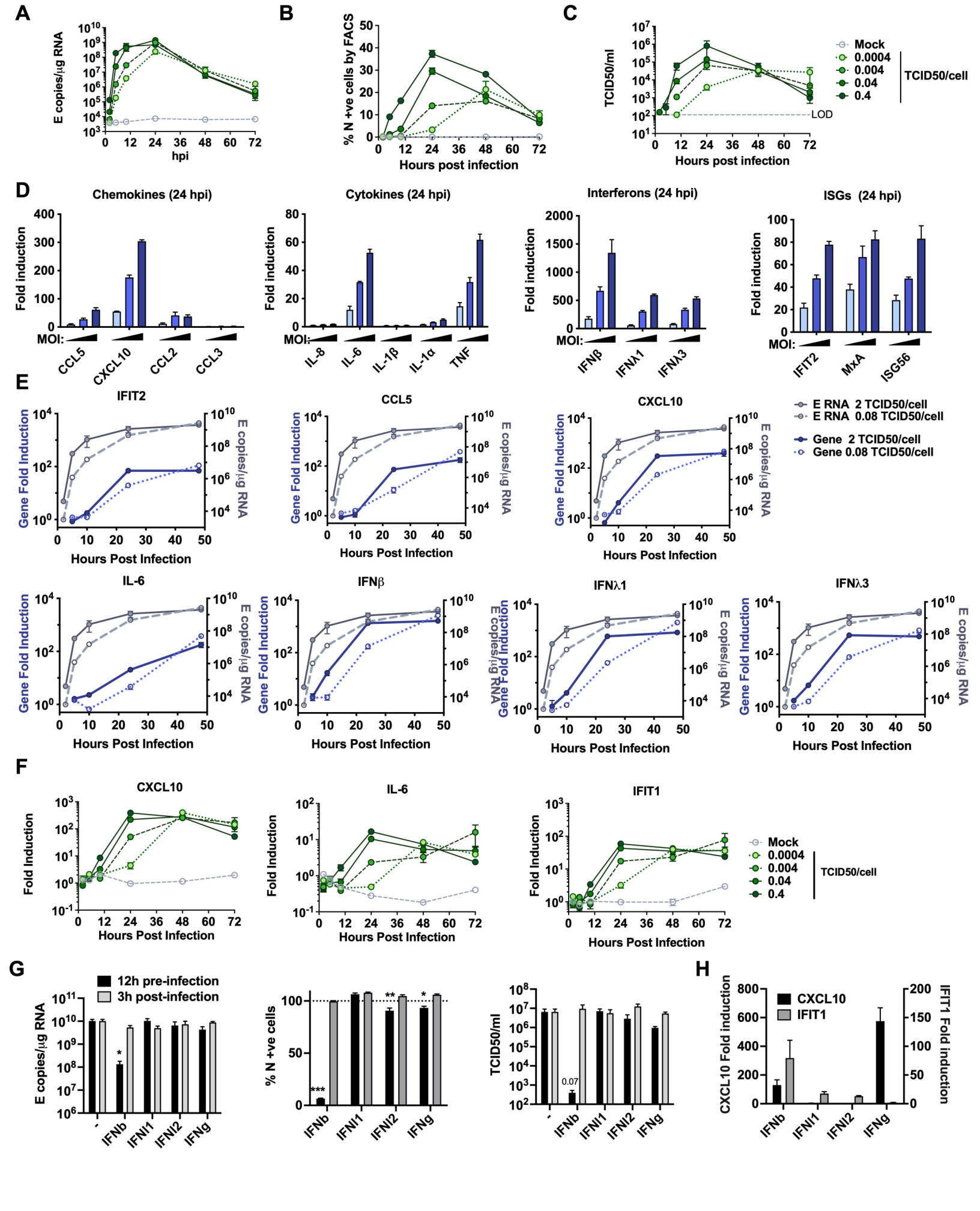
A
E copies/µg RNA
hpi
B
% N +ve cells by FACS
Hours post infection
C
TCID50/ml
Hours post infection
LOD
Mock
0.0004
0.004
0.04
0.4
TCID50/cell
D
Chemokines (24 hpi)
Cytokines (24 hpi)
Interferons (24 hpi)
ISGs (24 hpi)
Fold induction
MOI:
CCL5
CXCL10
CCL2
CCL3
IL-8
IL-6
IL-1β
IL-1α
TNF
IFNβ
IFNλ1
IFNλ3
IFIT2
MxA
ISG56
E
IFIT2
CCL5
CXCL10
IL-6
IFNβ
IFNλ1
IFNλ3
Gene Fold Induction
E copies/µg RNA
Hours Post Infection
E RNA 2 TCID50/cell
E RNA 0.08 TCID50/cell
Gene 2 TCID50/cell
Gene 0.08 TCID50/cell
F
CXCL10
IL-6
IFIT1
Fold Induction
Hours Post Infection
Mock
0.0004
0.004
0.04
0.4
TCID50/cell
G
12h pre-infection
3h post-infection
E copies/µg RNA
% N +ve cells
TCID50/ml
0.07
-
IFNb
IFNI1
IFNI2
IFNg
H
CXCL10
IFIT1
CXCL10 Fold induction
IFIT1 Fold induction

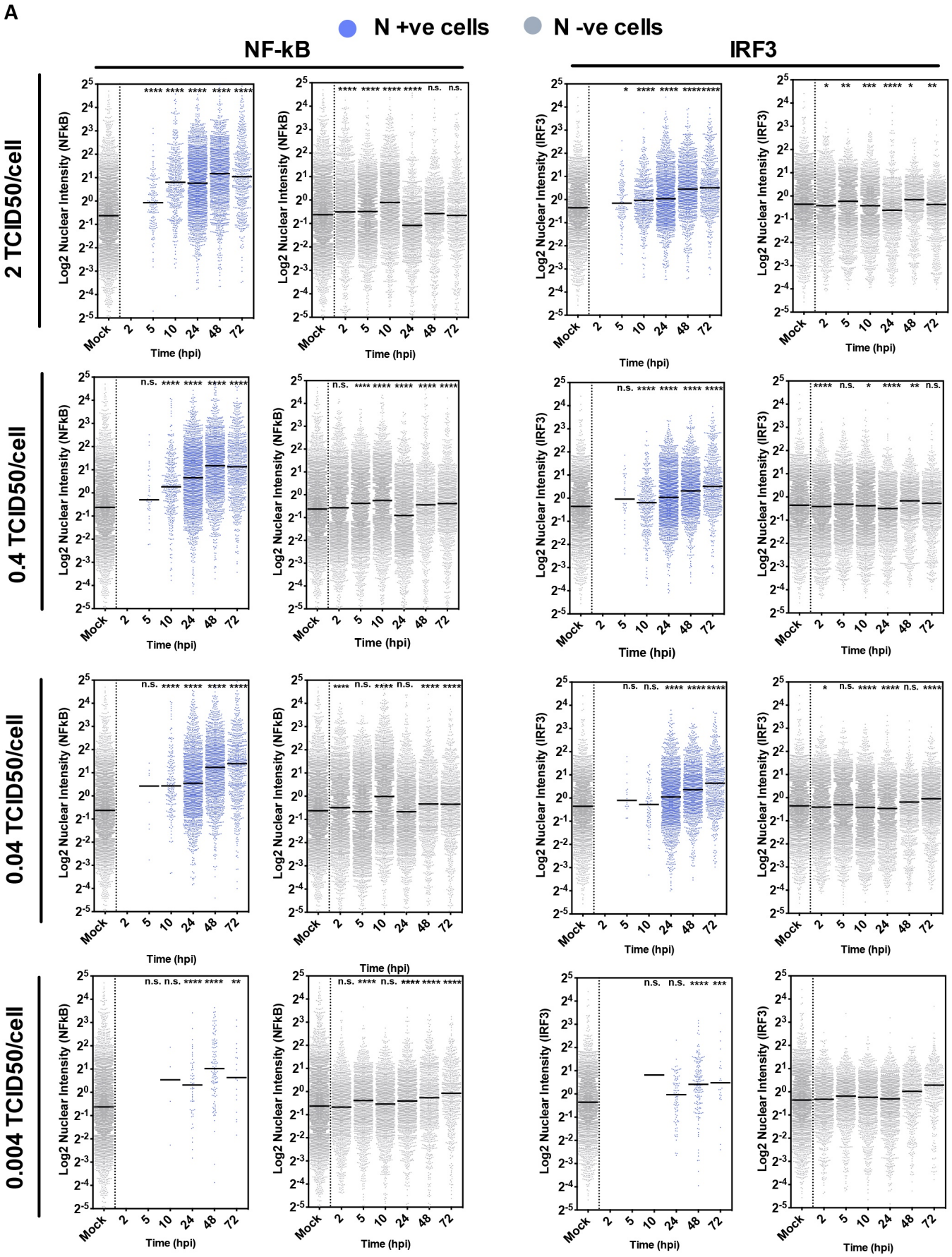
A
N +ve cells
N -ve cells
NF-kB
IRF3
2 TCID50/cell
0.4 TCID50/cell
0.04 TCID50/cell
0.004 TCID50/cell
Log2 Nuclear Intensity (NFkB)
Log2 Nuclear Intensity (IRF3)
Time (hpi)
Mock
2
5
10
24
48
72

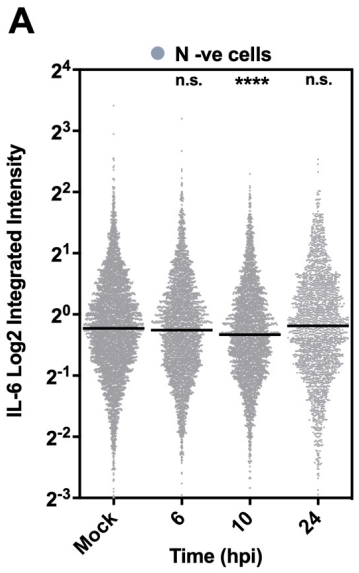
A
N -ve cells
n.s.
****
n.s.
IL-6 Log2 Integrated Intensity
Mock
6
10
24
Time (hpi)

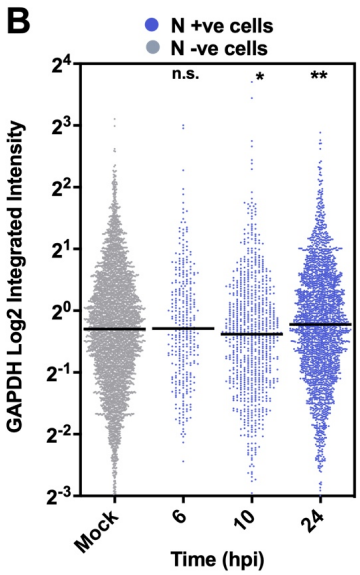
B
N +ve cells
N -ve cells
n.s.
*
**
GAPDH Log2 Integrated Intensity
Mock
6
10
24
Time (hpi)

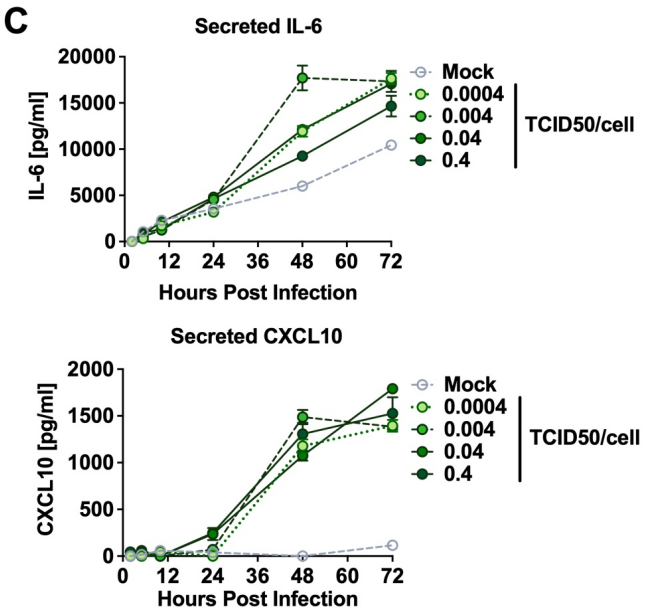
C
Secreted IL-6
IL-6 [pg/ml]
Hours Post Infection
Mock
0.0004
0.004
0.04
0.4
TCID50/cell
Secreted CXCL10
CXCL10 [pg/ml]
Hours Post Infection
Mock
0.0004
0.004
0.04
0.4
TCID50/cell

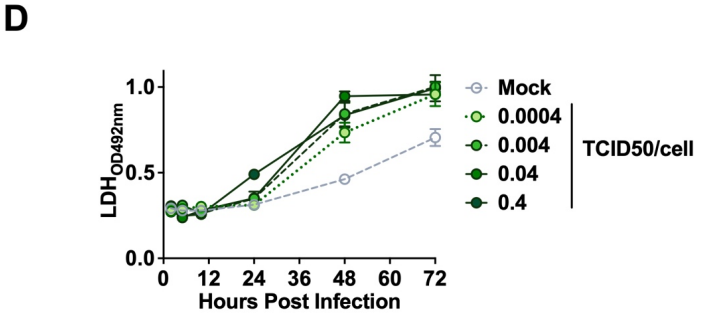
D
LDH OD492nm
Hours Post Infection
Mock
0.0004
0.004
0.04
0.4
TCID50/cell

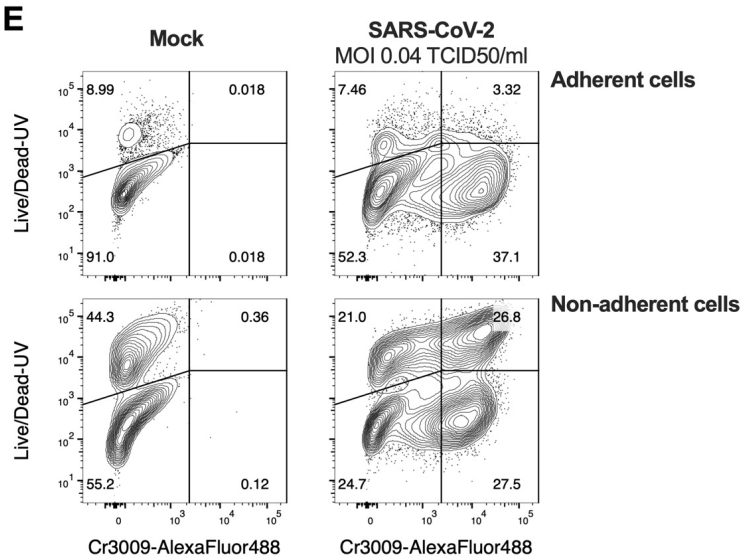
E
Mock
SARS-CoV-2
MOI 0.04 TCID50/ml
Adherent cells
Non-adherent cells
Live/Dead-UV
Cr3009-AlexaFluor488
8.99
0.018
91.0
0.018
7.46
3.32
52.3
37.1
44.3
0.36
55.2
0.12
21.0
26.8
24.7
27.5

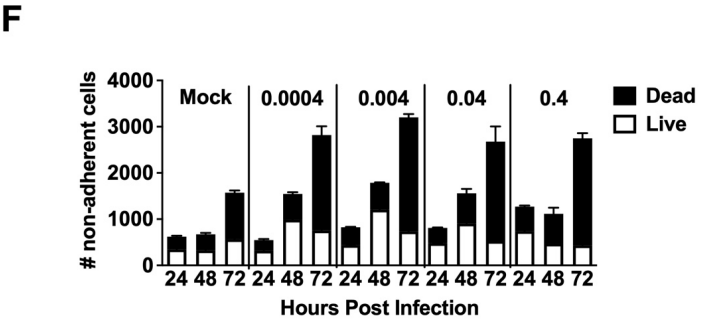
F
non-adherent cells
Mock
0.0004
0.004
0.04
0.4
Dead
Live
Hours Post Infection

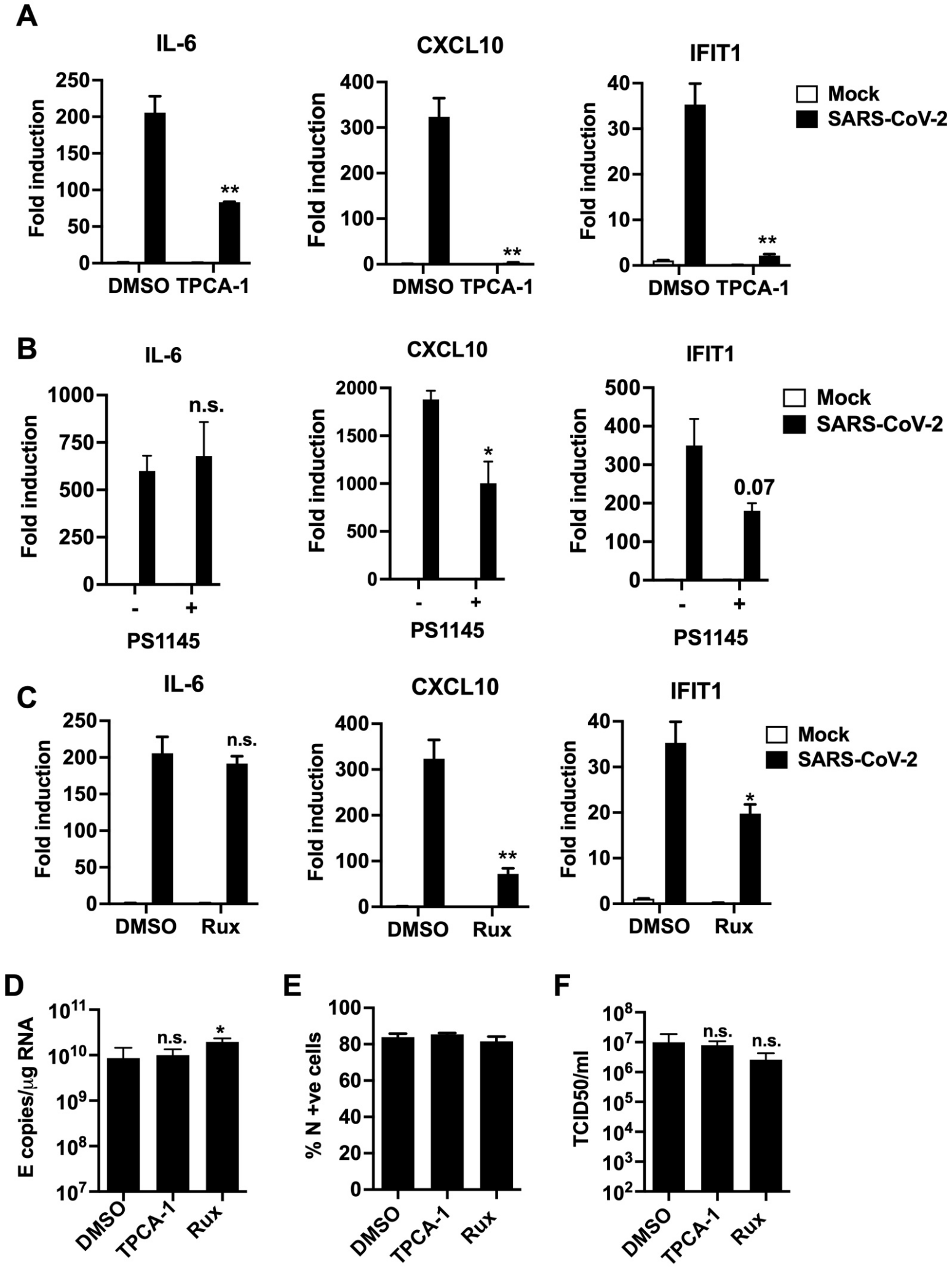
A
IL-6
CXCL10
IFIT1
Fold induction
Mock
SARS-CoV-2
DMSO
TPCA-1
**
B
n.s.
*
0.07
PS1145
C
Rux
D
E copies/μg RNA
n.s.
E
% N +ve cells
F
TCID50/ml